NASA Contractor Report 3027

Airframe Noise of the DC-9-31

A. B. Bauer and A. G. Munson

CONTRACT NAS1-14696
JULY 1978

NASA

NASA Contractor Report 3027

Airframe Noise of the DC-9-31

A. B. Bauer and A. G. Munson
Douglas Aircraft Company
Long Beach, California

Prepared for
Langley Research Center
under Contract NAS1-14696

National Aeronautics
and Space Administration

**Scientific and Technical
Information Office**

1978

CONTENTS

SUMMARY

Airframe noise measurements are reported for the DC-9-31 aircraft flown at several speeds and with a number of flap, landing gear, and slat extension configurations. The data are corrected for wind effects, atmospheric attenuation, and spherical divergence, and are normalized to a 1-meter acoustic range. The sound pressure levels are found to vary approximately as the fifth power of flight velocity. Both lift and drag dipoles exist as a significant part of the airframe noise. The sideline data imply that a significant side-force dipole exists only for the flap- and gear-down configurations; for others, the data imply the existence of only the lift and drag dipoles. The data are compared with airframe noise predictions using the drag element and the data analysis methods. Although some of the predictions are good, further work is needed to refine the methods, particularly for the flap- and gear-down configurations.

INTRODUCTION

Existing analytical methods for predicting airframe noise have been reviewed in a paper presented at the AIAA 3rd Aeroacoustics Conference (Reference 1). The methods can be grouped into three categories: (1) those that predict overall sound pressure levels for complete aircraft (References 2 and 3 and the clean airplane method of Reference 4); (2) those that predict overall sound pressure or spectra from gross parameters such as drag or component areas (Reference 5); and (3) those that predict aircraft component noise from local flow properties and noise models for the individual sources (the component analysis method of Reference 4). The conclusion drawn in Reference 1 was that flyover noise data would be useful to investigators trying to evaluate and possibly improve the methods of predicting airframe noise.

An analysis of DC-10 flyover noise data with engines at reduced power is given in Reference 1, which shows that data recorded with different microphones and from different flyovers are consistent within a reasonable experimental accuracy if spherical divergence and atmospheric attenuation are accounted for. A comparison of data from several different configurations shows that airframe noise was measured successfully up to a reasonable high frequency – 3150 Hz. Above this frequency, engine noise may be masking the airframe noise.

The directivity of the noise for any configuration could not be represented by a single dipole oriented in the lift direction. Instead, a lift and a drag dipole were required, a side-force dipole was sometimes required, and the combination represented the directivity of all configurations accurately. Since all flyovers were made at very nearly the same speed, no deduction for the variation in noise levels with velocity was possible.

A related study using the DC-9-31 airplane is reported on here. Flights were carried out with independent variations of slats, flaps, and landing gear; also, the testing was done over as large a speed range as was practical using the DC-9. Results for the various configurations are given this paper. Two airframe noise prediction methods, the drag element method (Reference 5) and the data analysis method (Reference 1), are discussed, and the results of a comparison of these methods with DC-9 flyover data are presented.

SYMBOLS

α	Angle of attack of fuselage reference plane
γ	Angle of flight path with respect to the horizon
θ	Aircraft attitude
λ	Acoustic range angle
μ	Sideline angle
a_i	See Equation (11)
a_o	Speed of sound
A_i	See Equation (6)
B_i	See Equation (7)
C_i	See Equation (8)
D_o D_2, D_m, E_2 E_m	Fourier series coefficients, Equations (A-2) through (A-5) in the appendix
f	Frequency
F_ℓ	Lift dipole dimensionless coefficient for 1/3 OB SPLs
F_d	Drag dipole dimensionless coefficient for 1/3 OB SPLs
$F_{\ell d}$	Lift-drag correlation, dimensionless coefficient for 1/3 OB SPLs
F_L	Lift dipole dimensional coefficient for 1/3 OB SPLs
F_D	Drag dipole dimensional coefficient for 1/3 OB SPLs
F_{LD}	Lift-drag correlation, dimensional coefficient for 1/3 OB SPLs
G	See Equation (9)

H	See Equation (3)
K_ℓ	Lift dipole dimensionless coefficient for OASPLs
K_d	Drag dipole dimensionless coefficient for OASPLs
$K_{\ell d}$	Lift-drag correlation, dimensionless coefficient for OASPLs
K_L	Lift dipole dimensional coefficient for OASPLs
K_D	Drag dipole dimensional coefficient for OASPLs
K_{LD}	Lift-drag correlation, dimensional coefficient for OASPLs
M	Mach number, V/a_o
M_r	$M \cos \lambda$
p_a	Atmospheric pressure
p_o	Acoustic reference pressure (20×10^{-6} P_a)
R	Acoustic range
R_g	Geometrical or optical range
S	Strouhal number, see Equation (12)
S_w	Wing reference area
V	Aircraft airspeed
X	Coordinate parallel to runway and in flight direction
Y	Coordinate in the horizontal direction, perpendicular to X, to pilot's left
Z	Coordinate in the vertical direction, perpendicular to X and Y

EXPERIMENTAL DATA BACKGROUND

Flyover noise measurements were recorded for eight combinations of flap deflection, landing gear position, and slat position with the engines of the aircraft at flight idle power. The configurations are identified by letters A through H, as indicated in Table 1. A three-view drawing of the aircraft is presented in Figure 1, and a more detailed description is given in Reference 6. In addition, Reference 6 gives the wind data, weather data, test procedure, microphone layout, flight path data, and a tabulation of the sound pressure level (SPL) time history for each of the eight microphones. The SPLs have been obtained by filtering the raw microphone data into 24 one-third octave bands (1/3 OBs) and by averaging over a 0.5 second time period. For five of the configurations, flyovers were performed at several different values of airspeed, as indicated in Table 2, so that a total of 18 runs were made at flight idle power. In addition, as indicated by Tables 1 and 2, three runs were made with the engine speed greater than flight idle so that engine effects could be studied.

The SPL data have been corrected for atmospheric attenuation by the method of Reference 7; the effect of spherical divergence has been accounted for by adding 20 log R to the data where R is the acoustic range (as used in Reference 1) so that the data are normalized to a 1-meter radius from the source. (For Reference 1, R was given in feet; hence, the numbers in Reference 1 should be decreased by 10.32 dB to convert them to the 1-meter radius convention.)

The definition and calculation of R may be best understood with the aid of Figure 2, which also serves to define the acoustic range angle λ and the sideline angle μ. A rectangular coordinate system, like that shown in Reference 6, was used where the X-axis is parallel to the (horizontal) runway and the

TABLE 1
CONFIGURATION LIST

Configuration	Flap Deflection (Degrees)	Gear	Slat Extension (Percent)	$\left(\frac{\text{Engine Speed}}{\text{Flight Idle}}\right)$
I	0	Up	0	1.1 to 1.3
A	0	Up	0	1.0
B	0	Down	0	1.0
C	0	Up	100	1.0
D	0	Down	100	1.0
E	20	Up	100	1.0
F	40	Down	100	1.0
G	40	Up	100	1.0
H	50	Down	100	1.0

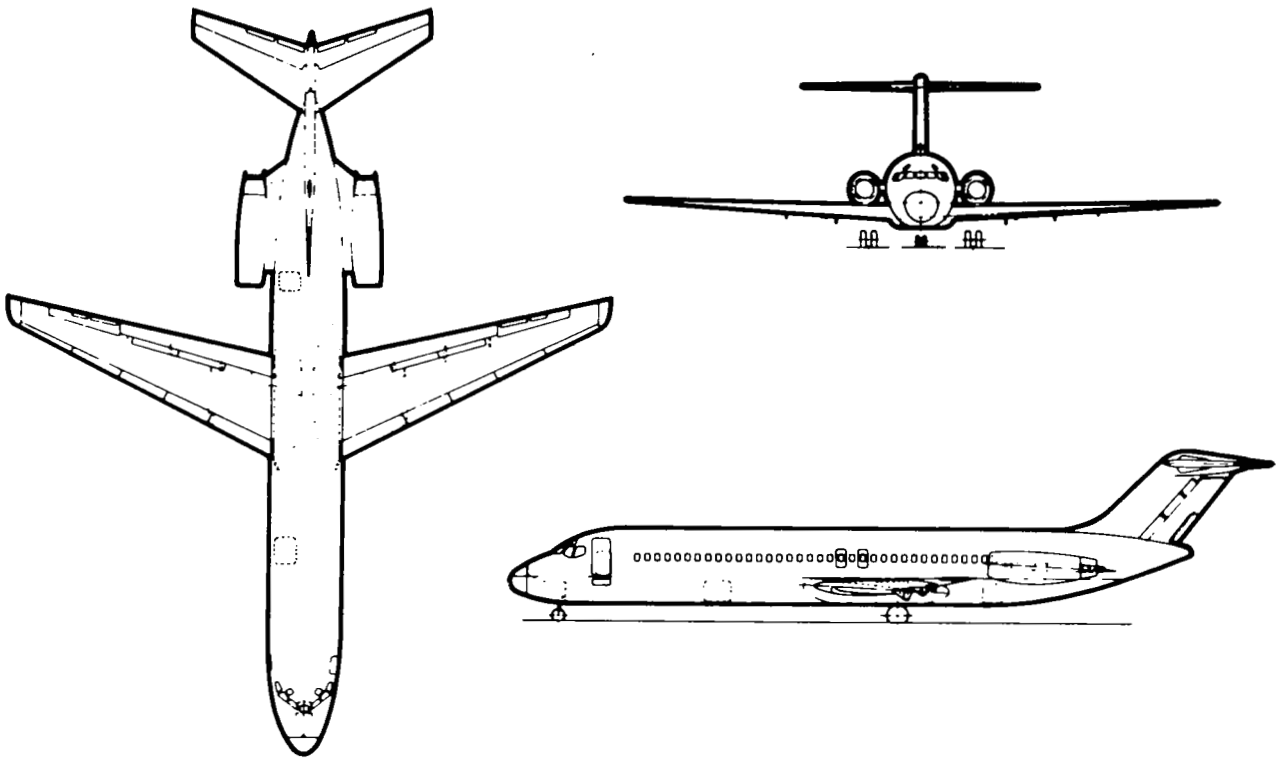

FIGURE 1. DC-9-31 AIRCRAFT

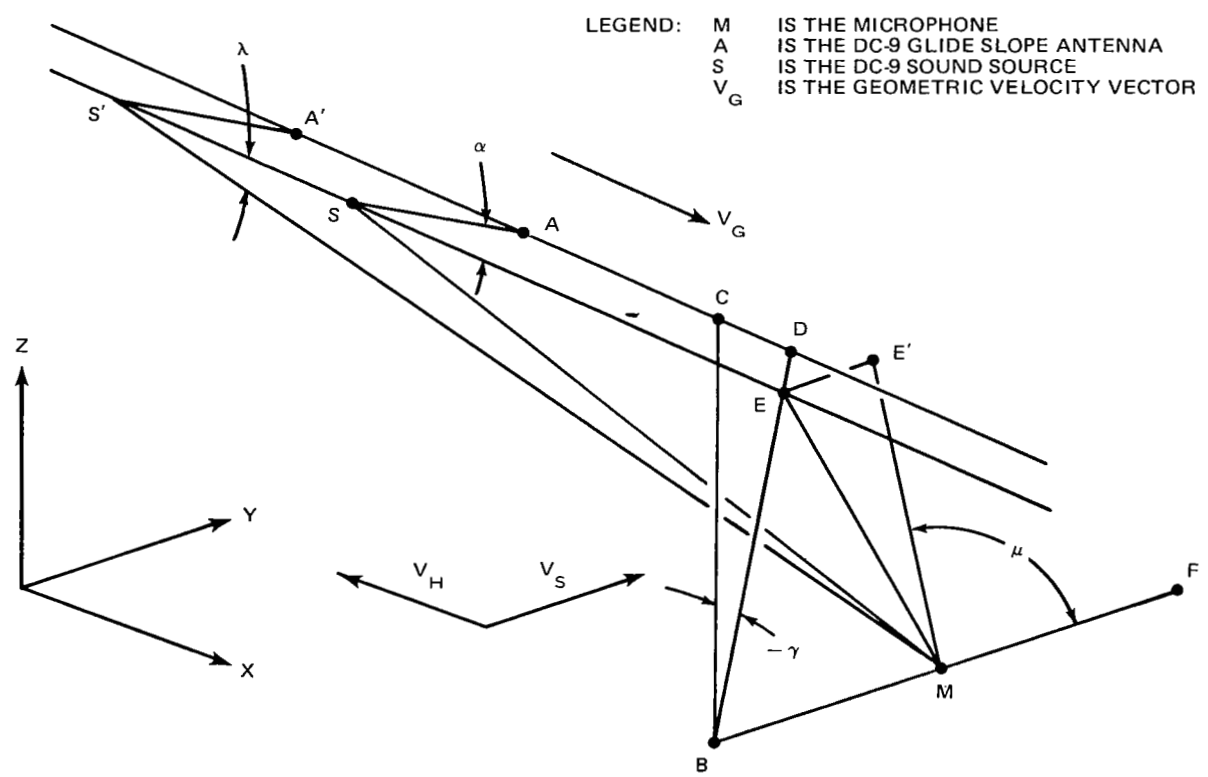

FIGURE 2. DEFINITION OF THE ACOUSTIC RANGE ANGLE λ AND THE SIDELINE ANGLE μ

TABLE 2
FLIGHT CONDITIONS

Configuration	Run No.	V (m/s)	W ($N/10^6$)	C_L	α (Deg)	γ (Deg)	θ (Deg)
I	3	115.0	0.395	0.536	4.6	- 2.4	2.2
I	4	114.8	0.392	0.530	4.5	- 2.7	1.8
I	6	114.4	0.389	0.528	4.5	- 2.6	1.9
A	7	111.0	0.382	0.550	4.8	- 2.6	2.2
A	9	108.4	0.404	0.591	5.3	- 3.6	1.7
A	11	130.8	0.391	0.400	3.0	- 4.4	- 1.4
A	17	151.2	0.396	0.296	1.8	- 6.3	- 4.5
B	16	110.5	0.384	0.538	4.7	- 6.5	- 1.8
B	24	149.3	0.353	0.267	1.4	-12.1	-10.7
B	25	151.5	0.349	0.256	1.2	-13.2	-12.0
C	8	90.2	0.379	0.826	9.0	- 3.7	5.3
C	10	106.9	0.401	0.602	6.4	- 4.4	2.0
D	22	129.2	0.360	0.368	3.6	- 8.4	- 4.8
E	13	80.5	0.394	1.041	5.8	- 5.4	0.4
E	15	93.6	0.388	0.754	2.8	- 7.1	- 4.3
E	23	117.0	0.356	0.441	-0.4	-10.7	-11.1
F	26	91.3	0.346	0.700	-1.0	-13.0	-14.0
G	27	79.1	0.343	0.925	-1.9	-12.9	-14.8
H	19	90.9	0.371	0.752	-3.8	-13.5	-17.3
H	20	80.6	0.367	0.953	-1.7	-12.0	-13.7
H	21	81.7	0.363	0.913	-2.0	-13.3	-15.3

nominal flight direction. The Y-axis is also horizontal. The acoustic range is defined (see Figure 2) by means of a microphone position, M, and the airplane flight path, assumed to be a straight line with velocity V_G in space and represented by points A′, A, C, and D in the figure. The line A′ACD is the path traveled by the aircraft ILS glide slope antenna which is located in the nose of the aircraft; the path coordinates are given in Reference 6. Since the aircraft noise source position is different from that of the ILS antenna, the source path is represented by the line S′SE in Figure 2. The line from A to S represents the distance from the aircraft ILS antenna to the source; line AS is inclined at angle α to the flight path.

Although airframe noise sources are actually located throughout the airplane, for convenience, only one point has been taken for defining S. Since the wing is a major contributor to airframe noise, the location selected is the intersection of the aircraft plane of symmetry with a line drawn between the trailing edge points at the mean aerodynamic chord locations on the right and left wing panels. This point is 18.9 meters (62 feet) from the ILS glideslope antenna, and the line AS is parallel to the fuselage reference plane. Hence, α is equal to the aircraft angle of attack.

The vertical plane defined by the flight path contains the points A,A′,B,C,D,E,S, and S′ in the figure. The line SM is the geometric range R_g (not to be confused with the geometric or optical range used in Reference 6, which corresponds to a line from A to M). SM is, of course, a function of time. At any given time, the acoustic signal arriving at M was emitted from point S′ at an earlier or retarded time corresponding to the time interval required for the sound to travel the distance S′M. S′M is defined as the acoustic range corresponding to the geometric range SM. (In Reference 6 the "acoustic range" is A′M.)

The line BC is vertical and defines the flyover "height" above the microphone used in Reference 6; BM is in the Y (horizontal) direction. The "lateral deviation" used in Reference 6 corresponds to the distance $(Y_B - Y_M)$, where Y_B and Y_M are the Y coordinates at B and M. Since the flyovers were performed at low power settings, the DC-9 lost altitude continuously during the flyovers, and the angle γ between the horizon and the flight path was always negative. Hence, the point of closest approach of A to M is at point D, so that ADB forms a right angle, and CBD is equal to $-\gamma$. Point E is the intersection of the source path and line BD, and the acoustic range angle λ is defined as ES′M. Hence, when $\lambda = 90$ degrees, which corresponds to the λ used for most of the data reduction used in this paper, S′ has advanced to E.

The last statement is strictly true only when the vertical flight path plane is parallel to the X direction, a condition that is sufficiently well satisfied for the flyover data considered in this paper.

The flyovers were complicated by the presence of wind, indicated in Figure 2 by a headwind velocity vector V_H (headed in the -X direction) and a sidewind vector V_S (headed in the +Y direction). Since V_H was small compared to the speed of sound, a, V_H was ignored for the purpose of computing R when λ was near 90 degrees. The sideline angle μ was first defined to be the angle EMF, but during the time that the acoustic signal travels the distance EM, V_S will move a particle from E to E′; hence the sideline angle μ was redefined to be the angle E′MF. The wind effect changed μ as much as 1.0 degree and the airspeed by 3 to 8 m/s.

AIRFRAME NOISE VARIATION WITH AIRSPEED

The overall sound pressure levels (OASPLs) measured under the flight paths and corrected for wind effects, atmospheric attenuation, and spherical divergence (by adding 20 log R) are plotted as a function of the airspeed V in Figure 3. Shown on the figure are data from Microphones 1G, 4G, 11G, and 12G; these were the ground-level microphones located almost directly under the flight paths so that μ was near 90 degrees. The restriction to microphones under the flight path was necessary because of variations observed in OASPLs as a function of μ. (See the section, Noise Variation With Sideline Angle.)

The corrected OASPLs for Configuration A, the "clean" configuration, show a variation with airspeed that is approximately proportional to V^5, particularly for Runs 7, 11, and 17 which cover the speed range of 111 to 151 m/s. The Run 9 data, for which V = 108 m/s, is the maverick run, a little above the V^5 line; this is the run for which Microphones 5G and 6G gave OASPLs lower than those from the other runs. (See the section, Noise Variation With Sideline Angle.) Because of an experiment problem, no noise was recorded by Microphones 1G and 4G during Run 9. Run 9 was also the first of the 19 runs carried out during Flight 105 on the second day of testing (Reference 6). Figure 3 shows that neither a V^4 nor a V^6 slope matches the Configuration A data as well as does the V^5 slope.

Figure 3 shows that Configurations B through H have considerably larger OASPLs than does Configuration A. The solid lines have a V^5 slope, and show that the configurations which have flyover data from two or more different airspeeds closely follow the V^5 trend. For Configuration B, Run 25 (151 m/s) is a little above the V^5 trend line, but Run 24 (149 m/s) is close to the line. From Figure 3 we conclude that the V^5 variation of OASPL is valid for the configurations which were tested. This is in agreement with the results of References 8 through 10 for aerodynamically clean configurations.

Since Configuration D has both gear and slats extended whereas Configuration B has only the gear extended and Configuration C has only the slats extended, one might expect that the Configuration D OASPLs would be above those for B or C. Figure 3 indicates that the opposite is true; D is slightly below B or C. Perhaps the aerodynamic wake from the slats may be affected by the flow over the gear to cause favorable interference and noise reduction; another reason for the apparent phenomena may be experimental data scatter. Only one run was made using Configuration D. A second run might have shown somewhat larger OASPLs.

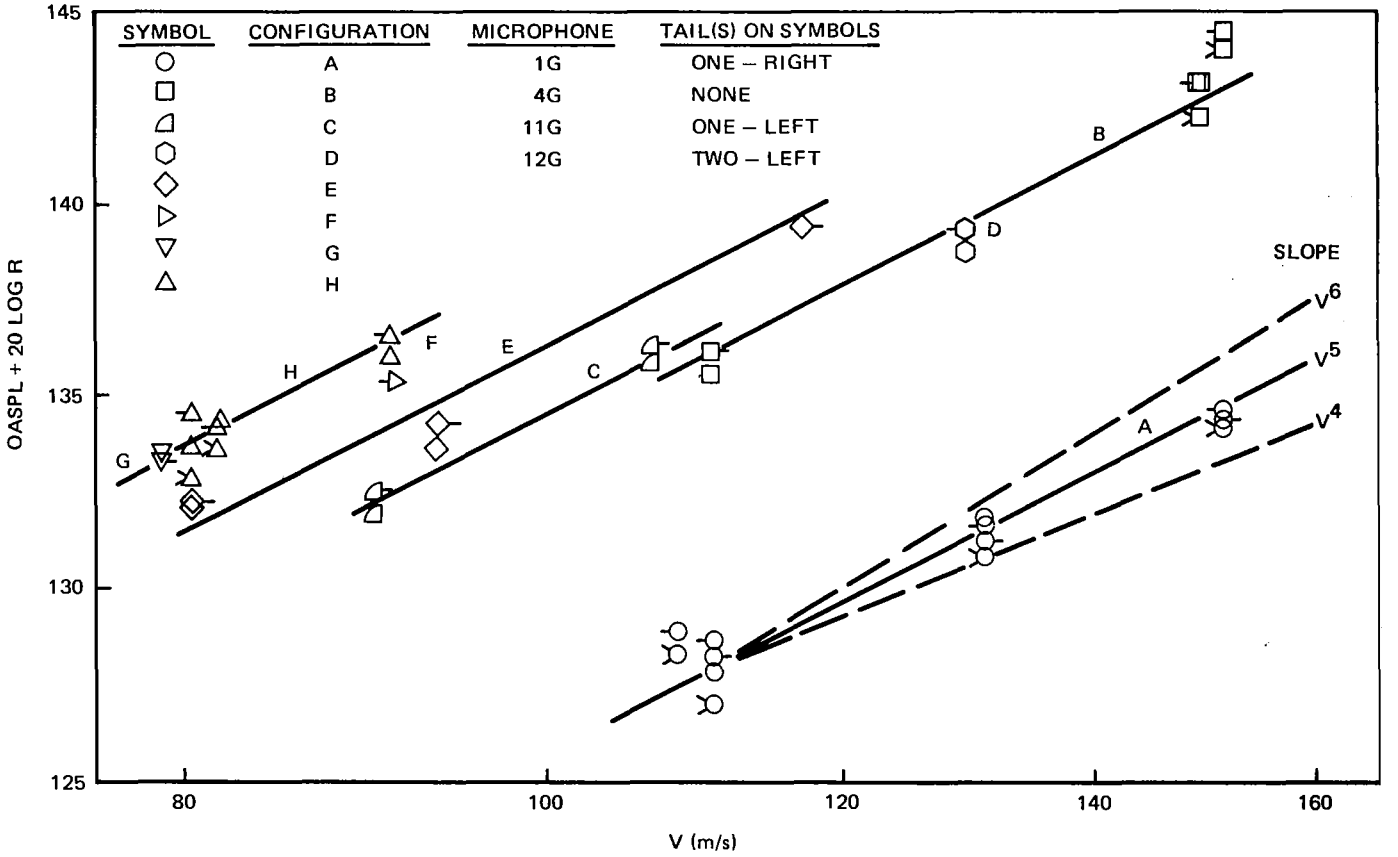

FIGURE 3. MEASURED OASPL'S CORRECTED FOR WIND SPEED, ATMOSPHERIC ABSORPTION, AND SPHERICAL DIVERGENCE, AIRPLANE OVERHEAD ($\mu \approx 90$ DEG) $\lambda = 90$ DEG

NORMALIZED SPL AND OASPL DATA

All the flyover airframe noise data presented hereafter, unless otherwise noted, have been normalized as follows:

1. The data have been corrected for atmospheric attenuation by using the rules in Reference 7.

2. The data have been corrected for spherical divergence to an acoustic range of 1 meter by adding 20 log R.

3. The data have been corrected for airspeed effects, using the V^5 power law, by adding 50 log (100/V) where V is airspeed in m/s. Hence, the data are normalized to a speed of 100 m/s.

The rules have been used both on individual 1/3 OB SPLs and on OASPLs obtained from 10 to 24 1/3 OBs.

EFFECT OF ENGINE NOISE

Some of the effects of increasing the engine speed above flight idle are shown in Figures 4 and 5, for which the OASPLs have been normalized as described earlier. The normalized OASPLs are computed using only the 1/3 OBs between 50 Hz and the band indicated by the abscissa of the figures. For example, the points having an abscissa of 3150 Hz represent the SPLs obtained by summing the noise in all the bands from 50 Hz through 3150 Hz. The data from Microphone 1G indicate that advancing the throttles from 1.0 to 1.2 times flight idle increases the SPLs by only about 0.3 dB for the range of frequencies below 3150 Hz; the higher frequencies are affected more by the engine speed increase. In contrast, a speed increase to 1.3 times flight idle gives a marked increase in SPL for all the frequencies shown on the figure. Results from Microphone 11G, shown in Figure 5, indicate similar trends. Figures 4 and 5 are done for the "clean" configurations. (Configurations A and I are clean and differ only by the engine speed settings.) Hence, a preliminary conclusion is that the engine noise at flight idle is not significant except for frequencies above 3150 Hz.

The data used to construct Figure 4 is shown in Figure 6 in the form of 24 one-third octave band SPLs. At frequencies below 2500 Hz, the SPLs for the runs with the throttles at 1.0, 1.1, and 1.2 times flight idle speed are so close together that only the 1.0 times flight idle run has been plotted, whereas the 1.3 times flight idle run has SPLs sufficiently large that the data could be plotted without crossing over the 1.0 times flight idle case. The data of Figures 4, 5, and 6 are all corrected to the condition of overhead flight (μ = 90 degrees) by the method given in the section titled Noise Variation With Sideline Angle, a needed procedure inasmuch as in Run 3 the data were taken with μ = approximately 77 degrees; later runs were taken with μ much closer to 90 degrees. Figure 6 clearly shows that the increases in SPL as engine speed is increased are most significant at frequencies above 3150 Hz.

Related data are shown in Figure 7, where SPLs are plotted for all 1/3 OBs and for various configurations. The data have been corrected only for atmospheric attenuation and to a common radius of 1 meter; hence, the engine and airframe noise is not normalized to an airspeed of 100 m/s. Figure 7 shows that the noise increases caused by going to Configurations B, C, or E were much larger than those caused by increasing the engine speed (Figure 6) for 1/3 OB frequencies up to 4000 Hz. At larger frequencies, the noise from the engine speed increases exceeds that caused by the configuration changes.

Figure 7 also shows noise data from ground testing the engines alone without the nacelles. Only one engine was tested; the data were raised by 3 dB to account for the noise of a second engine. Also, the ground test was done with the engine fixed in place so that no meaningful correction could be made to the data on the basis of V^5 for forward-flight effects. At frequencies above 2000 Hz, the bare-engine data are above those of Configuration A, partly because of the lack of a nacelle to quiet the engine.

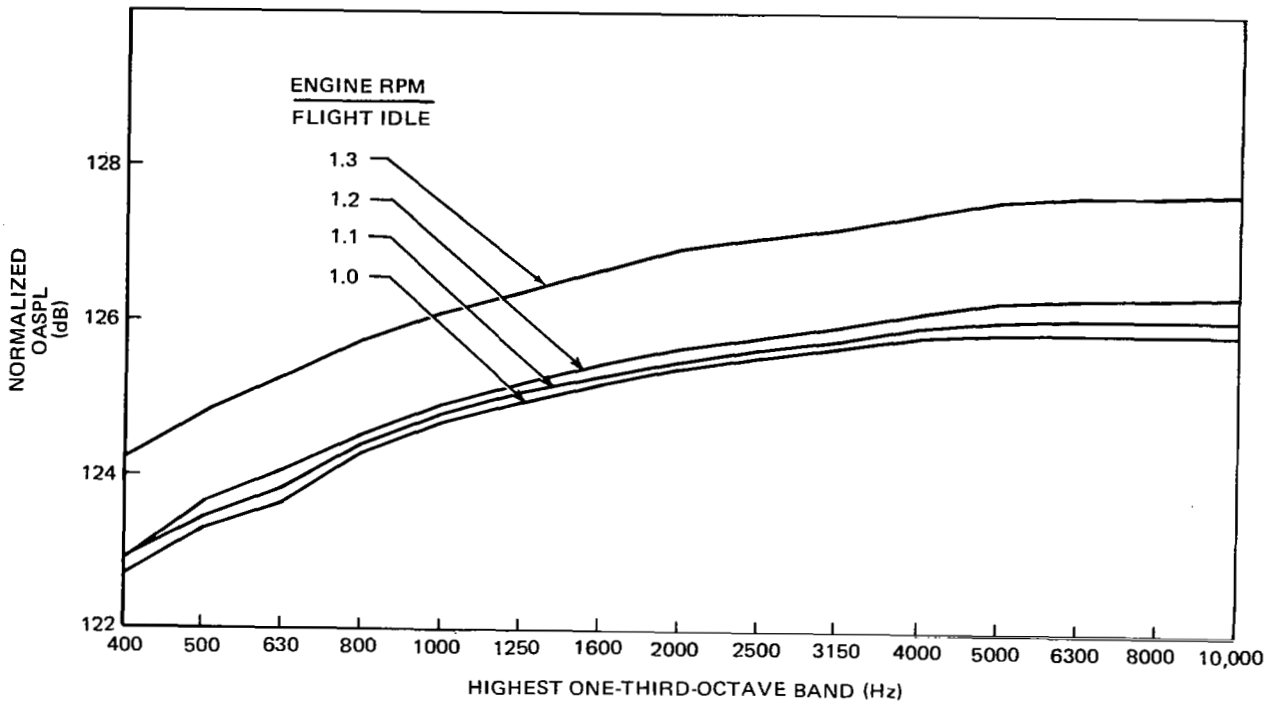

FIGURE 4. NORMALIZED OASPL MEASURED BY MICROPHONE 1G FROM RUNS 3, 4, 6, AND 7
λ = **90 DEG**
μ = **90 DEG**

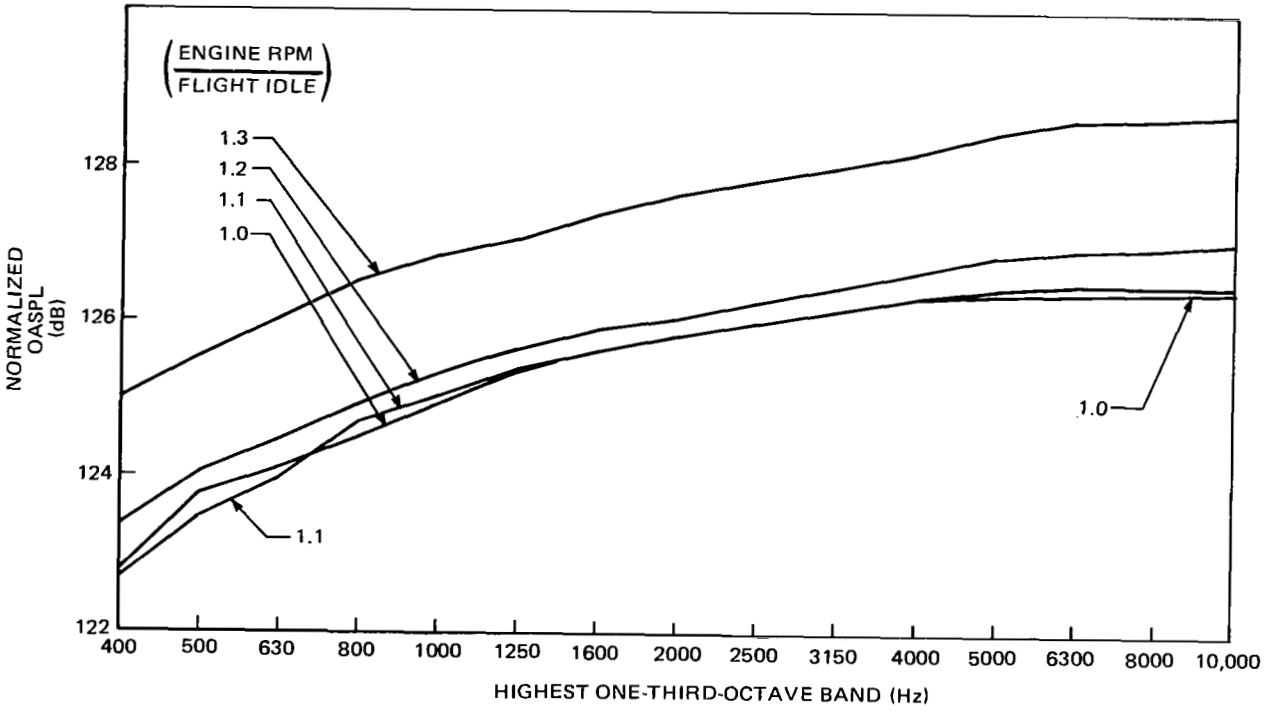

FIGURE 5. NORMALIZED OASPL MEASURED BY MICROPHONE 11G FROM RUNS 3, 4, 6, AND 7
λ = **90 DEG**
μ = **90 DEG**

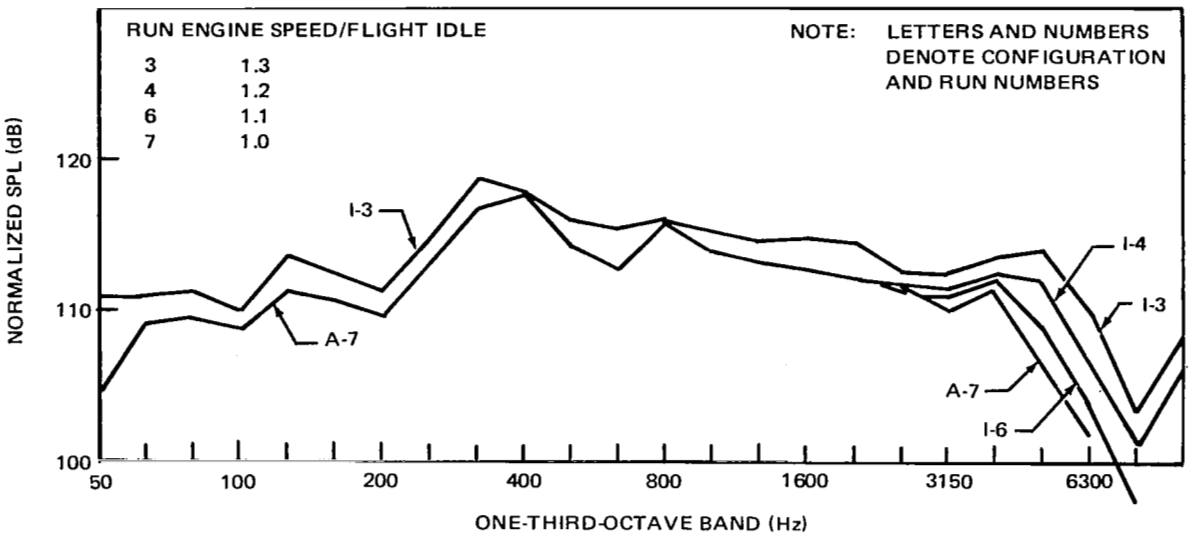

FIGURE 6. NORMALIZED SPL FROM MICROPHONE 1G (λ = 90 DEG, μ = 90 DEG)

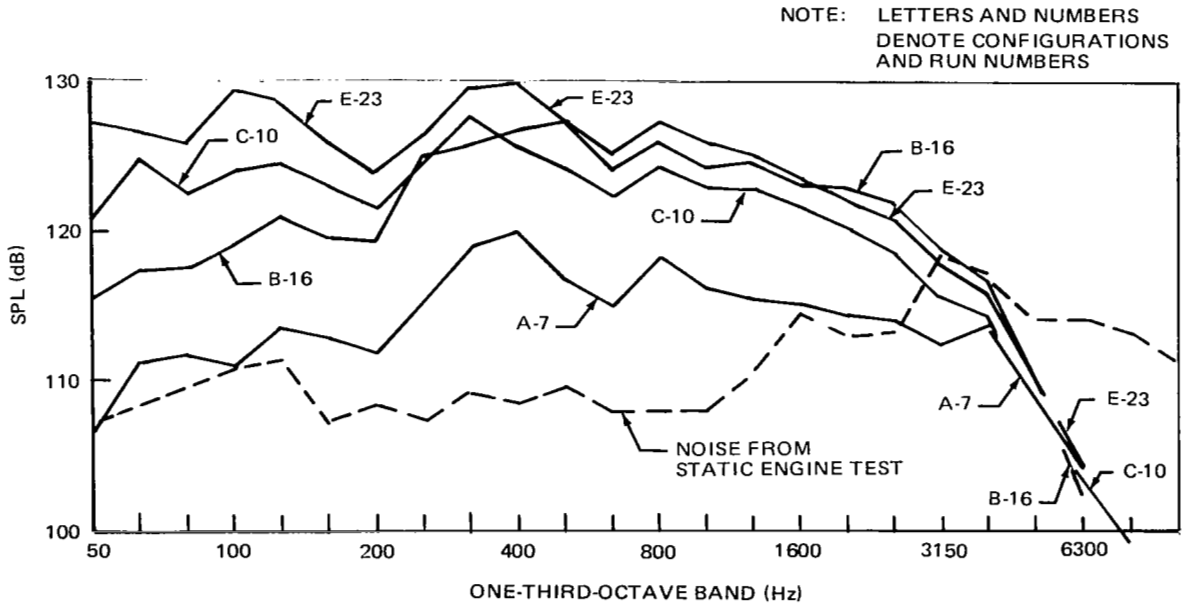

FIGURE 7. SPL CORRECTED FOR ATMOSPHERIC ATTENUATION AND AN ACOUSTIC RADIUS OF 1 METER FROM MICROPHONE 1G (λ = 90 DEG, μ = 90 DEG)

The above observations lead to the conclusion that at flight idle speed, the engine noise is significant only at frequencies above 3150 Hz. For Configuration A, the noise in the bands above 3150 Hz adds only about 0.4 dB to the OASPL; for Configurations B through H the effect of engine noise is much smaller.

DATA ANALYSIS METHOD FOR AIRFRAME NOISE PREDICTION

In Reference 1, Munson developed an airframe noise prediction method based on a modeling approach to an analysis of DC-10 airframe noise data. The method makes use of lift and drag dipoles and a correlation between the two dipoles to predict noise under the aircraft, but says nothing about sideline noise. The method is modified as shown below and will be referred to as the data analysis (DA) method.

In Reference 1, the expression for OASPL is

$$\text{OASPL} = 10 \log \left\{ \frac{V^6}{16 \pi^2 a_o^2 (1 - M_r)^4 R^2} \left[K_L \sin^2 \lambda + K_D \cos^2 \lambda + K_{LD} \sin \lambda \cos \lambda \right] \right\} \quad (1)$$

and the analogous expression for any 1/3 OB is

$$\text{SPL} = 10 \log \left\{ \frac{V^6}{16 \pi^2 a_o^2 (1 - M_r)^4 R^2} \left[F_L \sin^2 \lambda + F_D \cos^2 \lambda + F_{LD} \sin \lambda \cos \lambda \right] \right\} \quad (2)$$

where M_r is the relative Mach number, M cosλ.

It is also convenient for scaling purposes to render coefficients such as F_L dimensionless. This is best done by dividing the coefficient by

$$H = \frac{S_w p_a^2}{a_o^4 p_o^2} \quad (3)$$

where S_w is the aircraft wing area, p_a is the ambient atmospheric pressure, and p_o is the acoustic reference pressure (2×10^{-5} Pascals). Then, for the case $\lambda = 90$ degrees, we can write

$$\text{SPL} = 10 \log \left\{ \frac{M^5 S_w p_a^2}{16 \pi^2 R^2 p_o^2} \left(\frac{F_L M}{H} \right) \right\}$$

and by defining

$$F_\ell = \left(\frac{F_L M}{H} \right)^{1/2} \quad (4)$$

we have

$$SPL = 10 \log \left\{ \frac{M^5 S_w p_a^2 F_\ell^2}{16 \pi^2 R^2 p_o^2} \right\} \tag{5}$$

where M is the flight Mach number, V/a_o. The above manipulations were done for the purpose of transforming the dimensional coefficient into a dimensionless one which, assuming the V^5 power law to be correct, would not be a function of V or M. The 1/2 power of Equation (4) was used so that F_ℓ would have the form of a pressure coefficient (rather than a pressure-squared coefficient), and the p_o^2 factor was introduced because the definition of SPL is in the form of $10 \log (p/p_o)^2$ with p being the acoustic pressure. Of course, a_o is the obvious factor to use in nondimensionalizing V, and S_w was chosen as the best length-squared parameter needed for the nondimensionalization. S_w is used in the same fashion in References 5, 9, and 10.

In a fashion analogous to Equation (4), the other coefficients – K_L, K_D K_{LD}, F_D, and F_{LD} – may also be nondimensionalized. Then it is convenient to define the ratios

$$A_i = \begin{cases} \left(\frac{K_d}{K_\ell}\right)^2 & \text{for } i = 0 \\ \left(\frac{F_d}{F_\ell}\right)^2 & \text{for } i = \text{an integer} > 0 \text{ corresponding to a 1/3 OB} \end{cases} \tag{6}$$

$$B_i = \begin{cases} \left(\frac{K_{d\ell}}{K_\ell}\right)^2 & \text{for } i = 0 \\ \left(\frac{F_{d\ell}}{F_\ell}\right)^2 & \text{for } i = \text{an integer} > 0 \end{cases} \tag{7}$$

$$C_i = \begin{cases} K_\ell \text{ for } i = 0 \\ F_\ell \text{ for } i = \text{an integer} > 0 \end{cases} \tag{8}$$

$$G = \frac{M^{5/2} S_w{}^{1/2} p_a}{4\pi R (1 - M_r)^2 p_o} \tag{9}$$

Then for OASPL or for any designated one-third band, we have

$$SPL = 10 \log \left\{ G^2 C_i^2 (\sin^2 \lambda + A_i \cos^2 \lambda + B_i \sin \lambda \cos \lambda) \right\} \qquad (10)$$

Equation (10) is the nondimensional form of Equations (1) and (2), which are based on Reference 1, where the DC-10 airframe noise was modeled by accounting for the effect of convective amplification and by using lift and drag dipoles. Both lift and drag dipoles were found necessary to match the airframe noise data, and a negative correlation was found between the lift and drag dipoles.

The convective amplification or effect of the motion of the airframe on the noise level (the $(1 - M_r)$ term in Equations (1), (2), and (9)) is the subject of Reference 11. The author finds that the convective amplification has a strong effect on the source radiation, and that the lift dipole radiation pattern matches data much better than does that of a half-baffled dipole.

Figure 8 shows directivity patterns for lift and drag dipoles moving at Mach numbers of 0 and 0.3. The figure is drawn for a case where the ratio of drag dipole strength to lift dipole strength is 0.7 ($A_i = 0.7$) which is typical for 3 of the 4 DC-10 configurations reported in Reference 1.

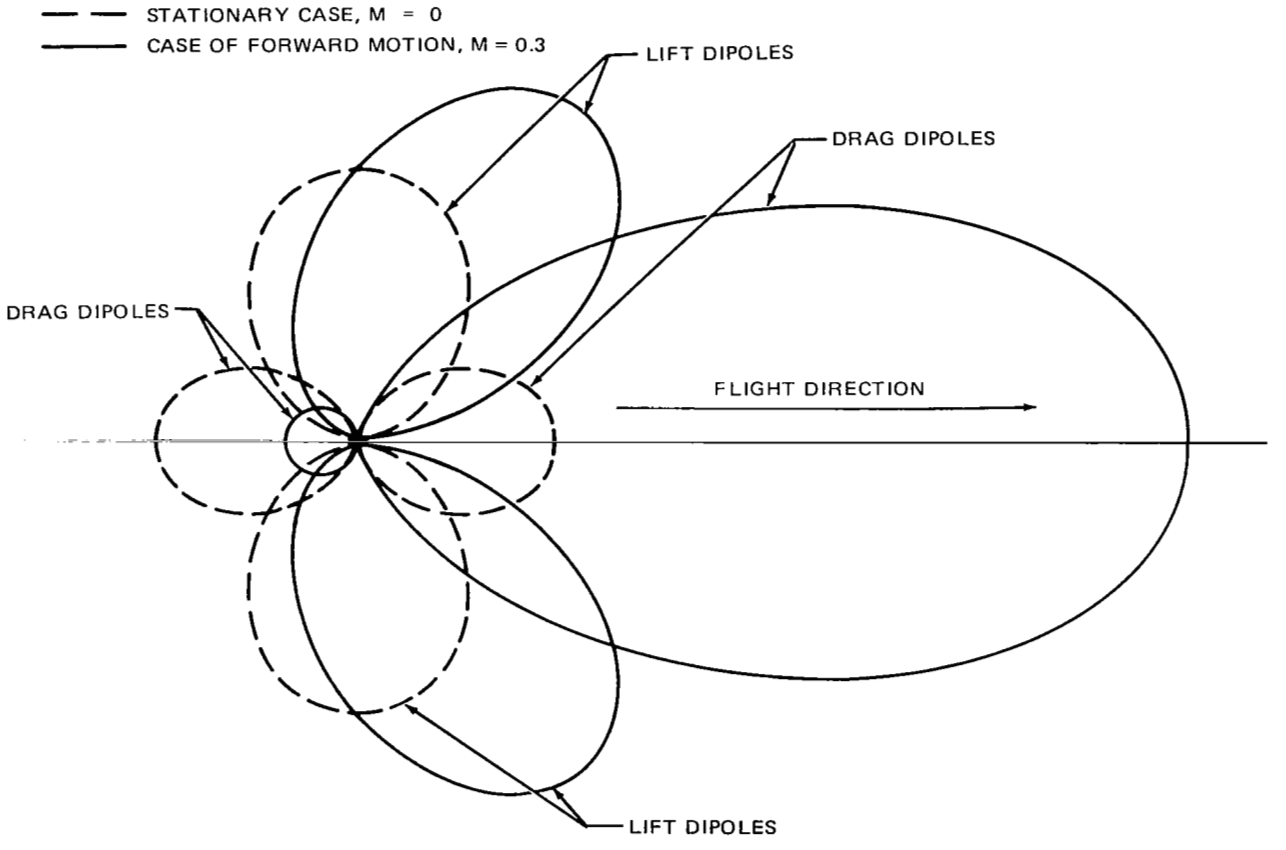

FIGURE 8. DIRECTIVITY PATTERNS FOR LIFT AND DRAG DIPOLES SHOWING THE EFFECT OF CONVECTIVE AMPLIFICATION

For sideline noise, we assume the existence of a side-force dipole which is uncorrelated with the lift or the drag dipoles. The fact that the airplane lift and drag are related implies a correlation between the lift and the drag dipoles, but there is no obvious relation between airplane lift and side force. The fact that the airplane and radiation pattern are symmetric about the aircraft centerline vertical plane also argues against such a relation. By including a side-force dipole in the derivation of Equations (6) through (9) of Reference 1, and then nondimensionalizing as shown above, the final result is

$$SPL = 10 \log \left\{ G^2 C_i^2 \left(\sin^2 \lambda \sin^2 \mu + A_i \cos^2 \lambda + B_i \sin \lambda \cos \lambda \sin \mu + a_i \sin^2 \lambda \cos^2 \mu \right) \right\} \qquad (11)$$

where a_i is the ratio of the strength of the side-force dipole to that of the lift dipole. Equation (11) is the general form of the DA method used to match airframe noise data.

The DA method may be used to predict the airframe noise of the DC-9 or any other aircraft by first calculating the nondimensional coefficients from the data of some aircraft test (e.g., the DC-10 data from Reference 1). Then, the coefficients may be used in Equation (11) to predict airframe noise. This, of course, assumes that the coefficients of both aircraft are alike, which is not strictly true unless both aircraft are geometrically similar and have related flow fields. However, as a practical matter we expect that aircraft which are not greatly dissimilar in geometry will have approximately the same coefficient.

Since the DC-10 and the DC-9 aircraft show marked differences in geometric shape, the use of DC-10 coefficients to predict DC-9 noise should be expected to produce only approximate results.

The DA method is not complete without the consideration of frequency scaling; that is, the coefficients such as F_ℓ must be taken to be functions of Strouhal number S where

$$S = \frac{f S_w^{1/2}}{a_o} \qquad (12)$$

and f is the band frequency. That is,

$$F_\ell = F_\ell(S) \qquad (13)$$

Hence, the DA method is a scaling method based on dimensionless parameters corresponding to the lift and drag dipole coefficients derived in Reference 1 and on a dimensionless parameter corresponding to a side-force dipole strength. Coefficients for a wide range of aircraft experimental data have not yet been tabulated. Such work is needed to either show the utility of the form given by Equation (11) or to serve as a basis for an improved airframe noise model.

NOISE VARIATION WITH ACOUSTIC RANGE ANGLE

The DC-9-31 airframe noise variation with acoustic range angle for Configuration A is shown in Figures 9 and 10; the data are from Runs 11 and 17, respectively. For $\lambda = 90$ degrees, the data from the two runs are in agreement, but for λ in the range of 120 to 150 degrees, the data from Run 11 are significantly greater than the data from Run 17. Evidently, the difference is partly the result of the convective amplification effect (the term $(1 - M_T)^2$ in Equation (9)) since the two runs are at different Mach numbers, and partly the result of the different lift-drag relations since the two runs are at different lift coefficients (see Table 2).

The shapes of the OASPL-versus-λ curves depend on the coefficients A_0 and B_0, assuming Equation (11) to be a valid airframe noise model. If both A_0 and B_0 are zero, only the lift dipole would be observed as the aircraft flys over the microphone. The situation is represented by Curve A in Figure 11, which was computed for $M = 0.45$ so as to match Figure 10. However, Curve A has a different shape than the curve of Figure 10. When A_0 is changed to 0.7, the model generates Curve B, which is tangent to Curve A at $\lambda = 90$ degrees, but the slope of Curve B at $\lambda = 90$ degrees is different than indicated by the data in Figure 10. Notice that M determines the slope through Equations (9) and (11). By changing B_0 to -1.0, Curve C is generated, and the slope of Curve C at $\lambda = 90$ degrees does match that of Figure 10. As may be seen in Equation (11), A_0 and B_0 control the shape of the curve in two different ways, and Curve C in Figure 11 is a good match to the data of Figure 10. The reason that the OASPL in Figure 10 decreases as λ decreases from 40 to 20 degrees is due to the fact that the aircraft is so far from the microphone that some of the 1/3 OB SPLs are close enough (5 dB) to the ambient noise levels that the data have been deleted; hence, the data for $\lambda < 40$ degrees is invalid. The data support the conclusion that both lift and drag dipoles exist, and that a correlation exists between them.

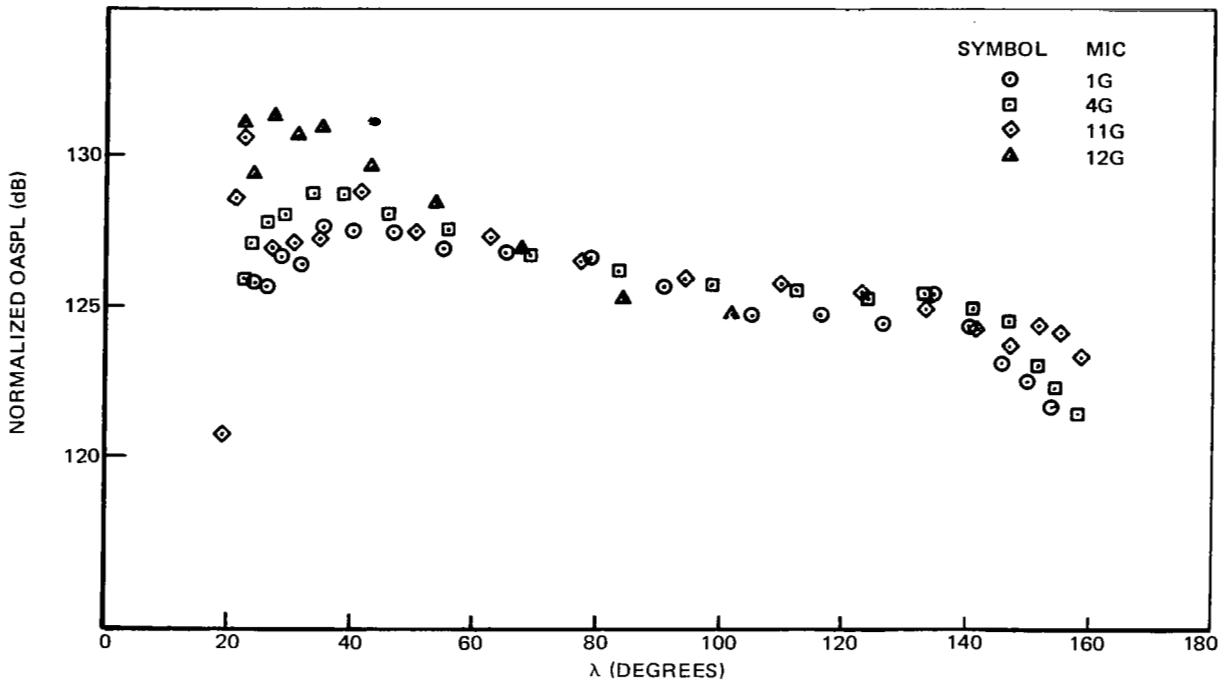

FIGURE 9. NORMALIZED OASPL VERSUS ACOUSTIC RANGE ANGLE DATA FROM CONFIGURATION A, RUN 11 ($\mu \approx 90$ DEG, M = 0.39)

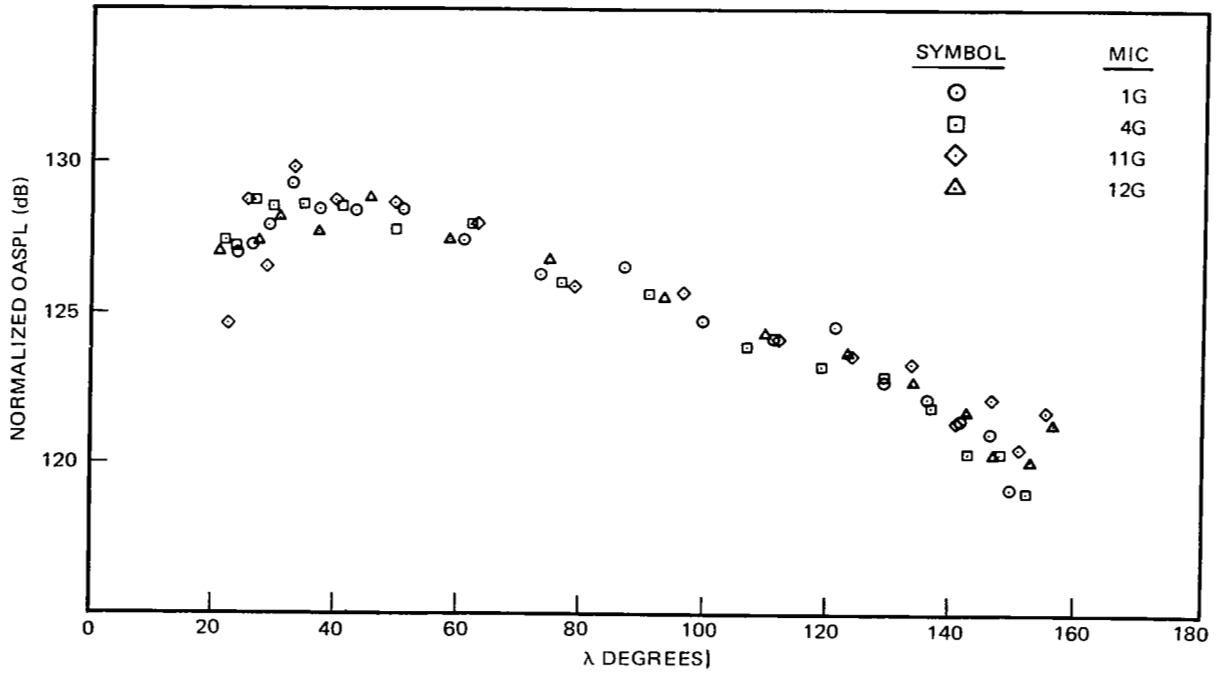

FIGURE 10. NORMALIZED OASPL VERSUS ACOUSTIC RANGE ANGLE DATA FROM CONFIGURATION A, RUN 17 ($\mu \approx 90$ DEG, M = 0.45)

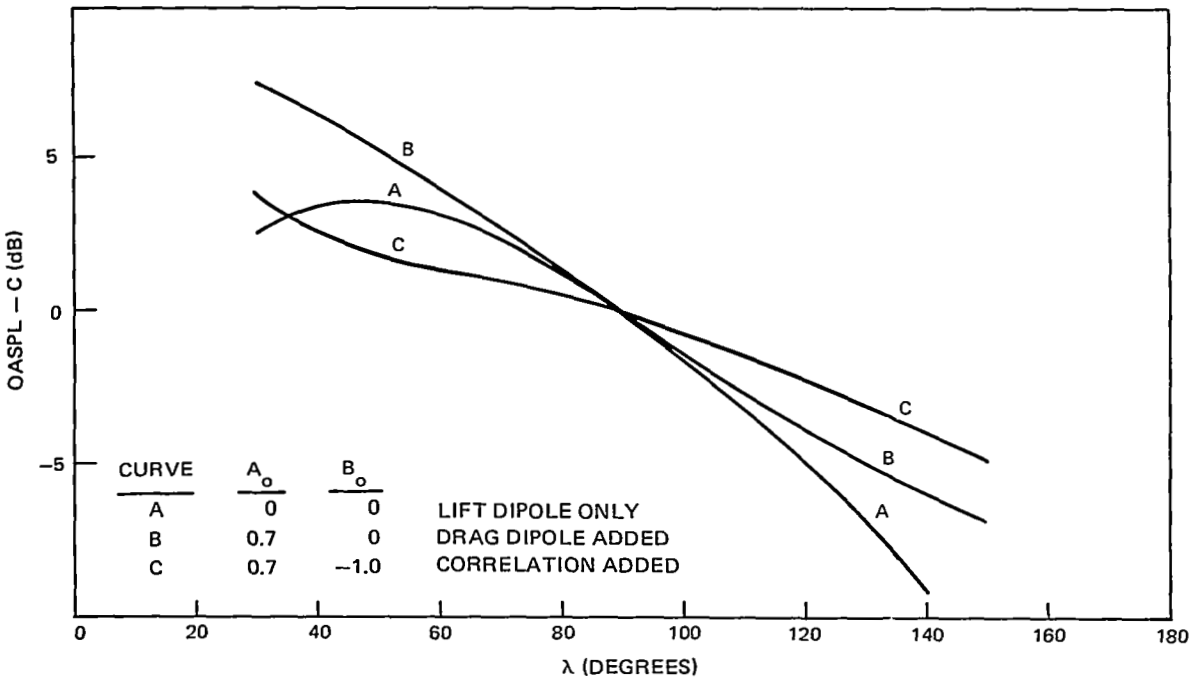

FIGURE 11. PREDICTED OASPL VARIATION WITH ACOUSTIC RANGE ANGLE FOR VARIOUS DIPOLE CONFIGURATIONS (μ = 90 DEG, M = 0.45)

NOISE VARIATION WITH SIDELINE ANGLE

The normalized OASPLs for Configurations A through H are given in Figures 12 through 19, respectively, for an acoustic range angle of 90 degrees and as a function of μ. In each figure, a curve in the form of a lift dipole,

$$\text{OASPL} = 10 \log \sin^2\mu + \text{constant},$$

is shown as a dashed line (see Equation 11 for the special case $\lambda = 90$ degrees and $a_i = 0$), with the constants adjusted for the best match to the data; in particular, the data match for μ near 90 degrees was given the most weight since the existence of any side-force dipole ($a_i > 0$ in Equation (11)) might be indicated by a deviation of the data above the lift dipole curve as μ moves away from 90 degrees.

Figure 12 shows that the lift dipole function is matched rather well by data from Runs 7, 11, and 17, but as mentioned earlier, Run 9 data are different. Figure 13 shows that the data for Runs 16 and 24 are reasonably consistent but that the Run 25 data are high compared with the others, especially in the case of Microphone 4G which gives a much larger OASPL value than do Microphones 11G and 12G. In general, the data follow the dipole trend rather well, but scatter exists in the data.

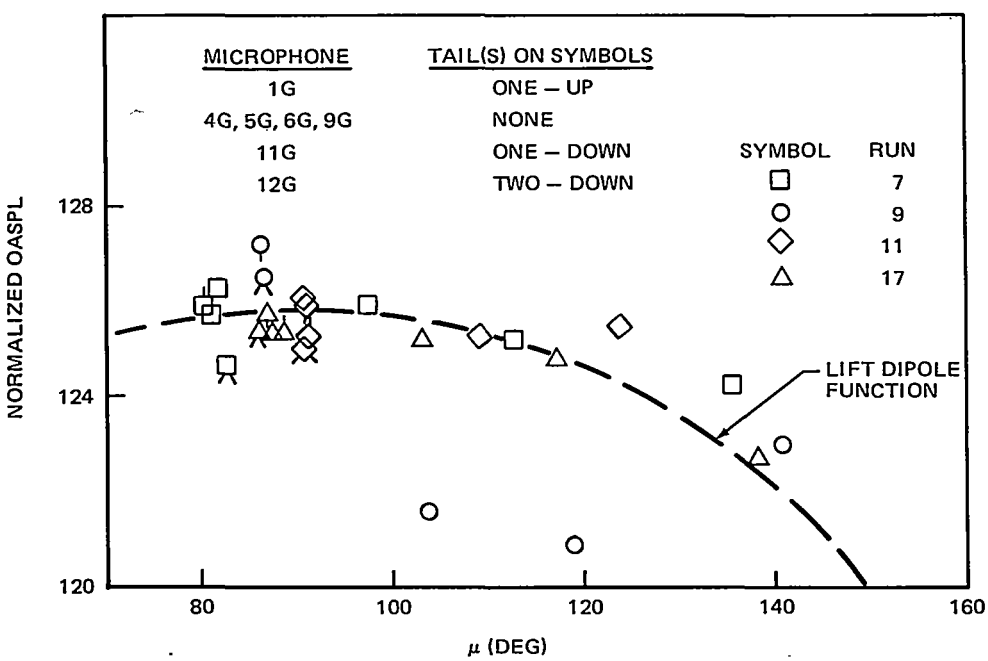

FIGURE 12. NORMALIZED OASPL FOR CONFIGURATION A
λ = 90 DEG

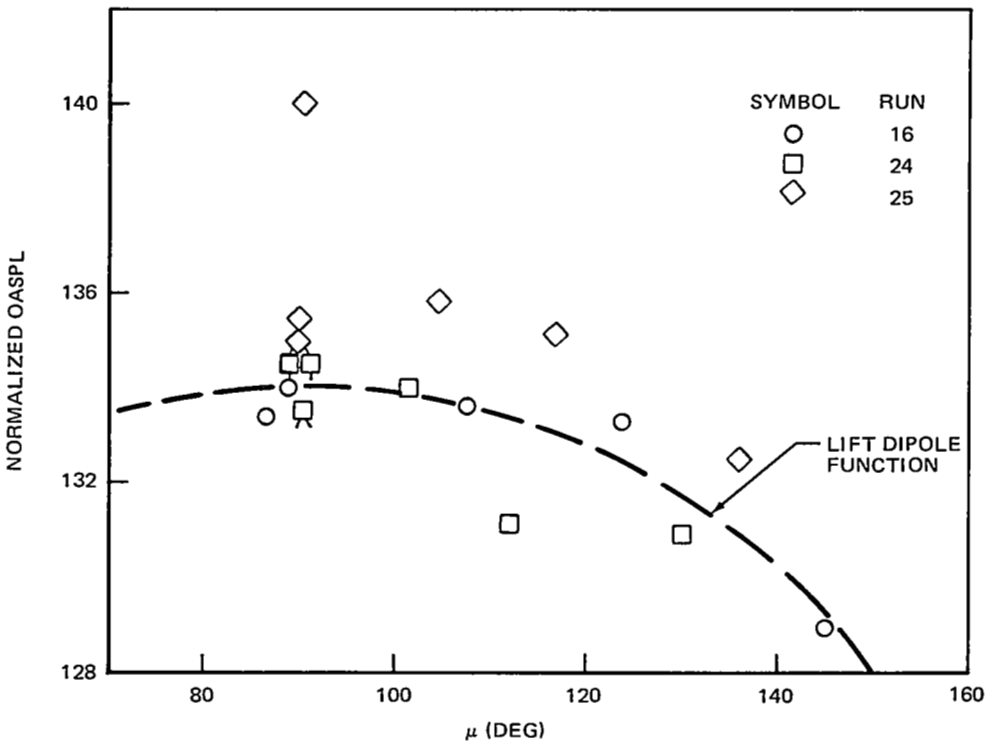

FIGURE 13. NORMALIZED OASPL FOR CONFIGURATION B
λ = 90 DEG

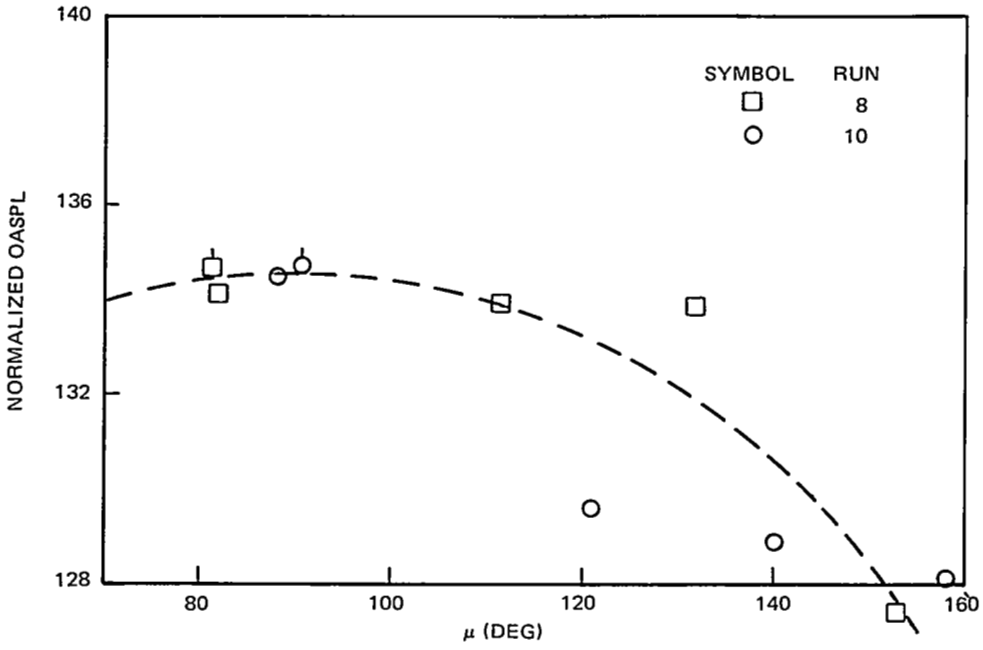

FIGURE 14. NORMALIZED OASPL FOR CONFIGURATION C
λ = 90 DEG

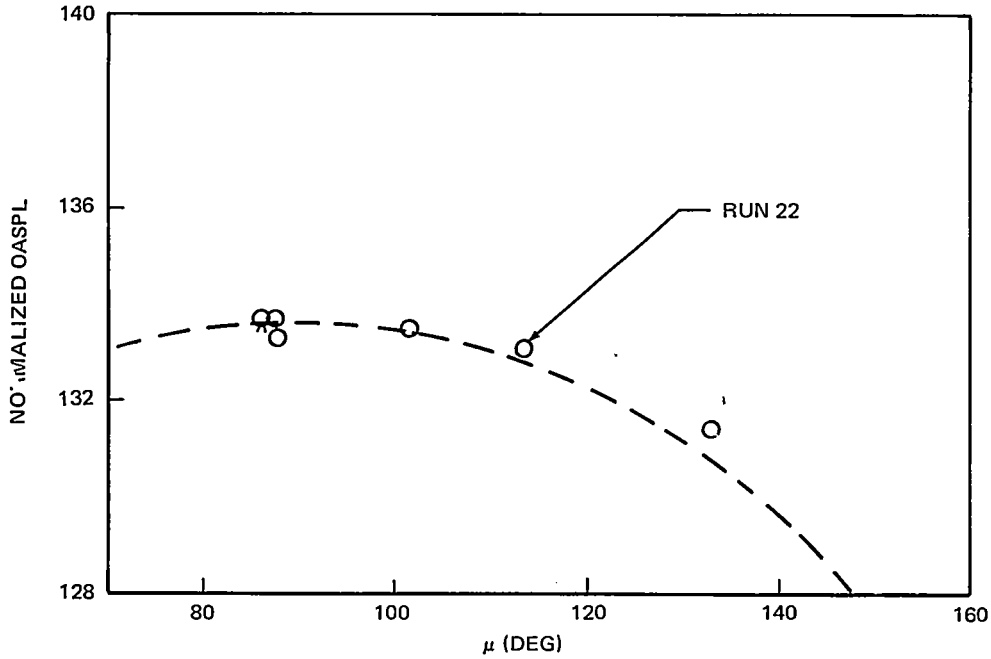

FIGURE 15. NORMALIZED OASPL FOR CONFIGURATION D
λ = 90 DEG

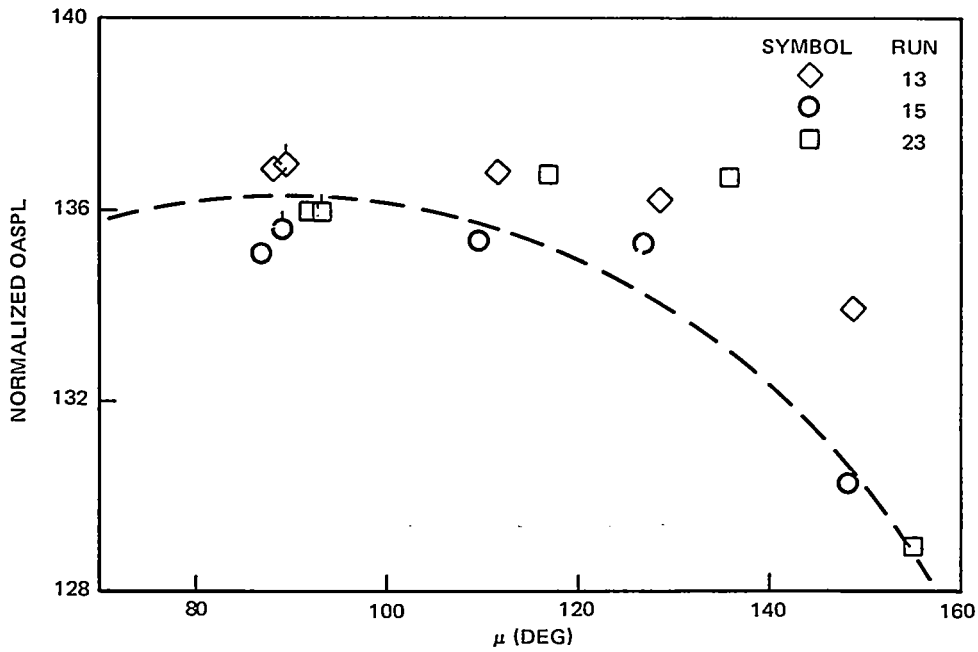

FIGURE 16. NORMALIZED OASPL FOR CONFIGURATION E
λ = 90 DEG

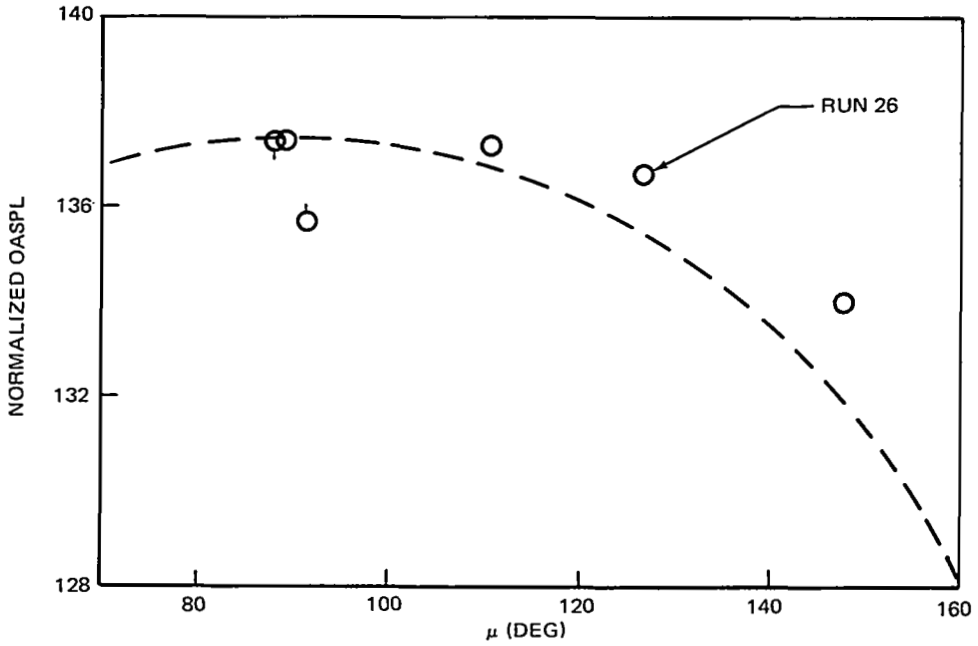

FIGURE 17. NORMALIZED OASPL FOR CONFIGURATION F
λ = 90 DEG

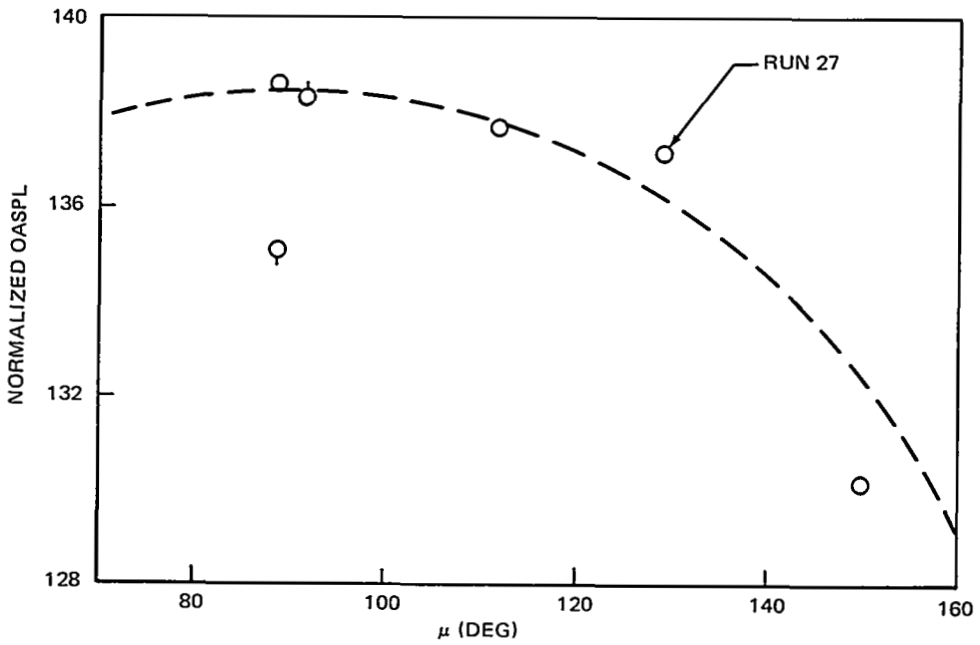

FIGURE 18. NORMALIZED OASPL FOR CONFIGURATION G
λ = 90 DEG

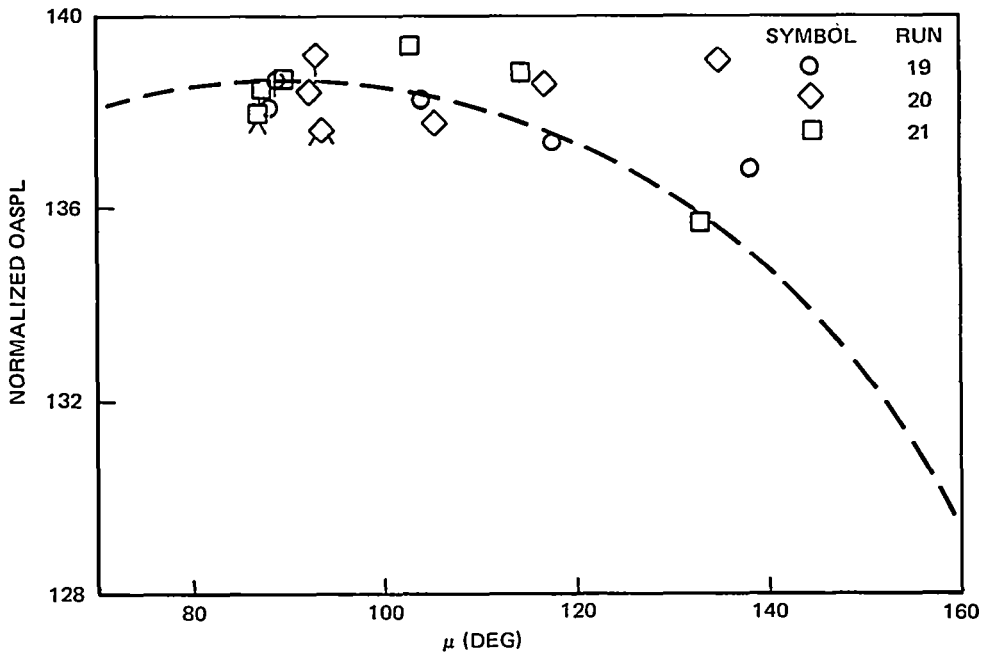

FIGURE 19. NORMALIZED OASPL FOR CONFIGURATION H
λ = 90 DEG

Although the normalized OASPLs in Figures 12 through 19 tend to vary like the lift dipole function (as plotted in each figure), examination of Figures 15, 17, and 19 shows that the data wander a little above the lift dipole trend as μ becomes large. This is indicative of a significant side-force dipole effect for Configurations D, F, and H, which are related in the fact that they are all gear-down configurations. Among all the other configurations, only B has the gear down, but the data from this configuration (Figure 13) show no obvious tendency to deviate from the lift dipole shape. The data for Configuration D show only a slight side-force dipole effect, which should be viewed with obvious caution since the apparent effect is smaller than the scatter in most of the DC-9-31 flyover noise data. So the side-force dipole effect, if any, is rather weak for the flaps-up gear-down Configurations B and D; but the flaps-down gear-down Configurations F and H show by the flight data a more significant side-force dipole effect. The large flap deflections of Configurations F and H place the flap close to the lowered main landing gears, hence the association of a side-force dipole with Configurations F and H is perhaps related to the landing gear flow field as modified by flap deflection.

The ratio of a side-force dipole energy to a lift dipole energy is denoted by a_i (Equation (11)) where, for any given frequency of dipole action, the phase of the lift and the side-force dipoles are assumed to be uncorrelated. The function

$$f(\mu, a_i) = 10 \log (\sin^2 \mu + a_i \cos^2 \mu)$$

is plotted in Figure 20. By comparing the data of Figure 20 with those of Figures 17 and 19, a measure of the magnitude of the side-force dipole has been obtained. The data imply that a_i is about 0.3 for Configuration F and about 0.4 or larger for Configuration H. Hence, the trend apparent from the data is that the side-force dipole appears for the gear-down configurations and becomes of significant strength as the flaps are lowered to their full-down position.

The matching of the dipole functions to the data has been used as an aid in estimating the true normalized OASPL for overhead flight ($\lambda = \mu = 90$ degrees). The OASPLs are shown in Table 3. The

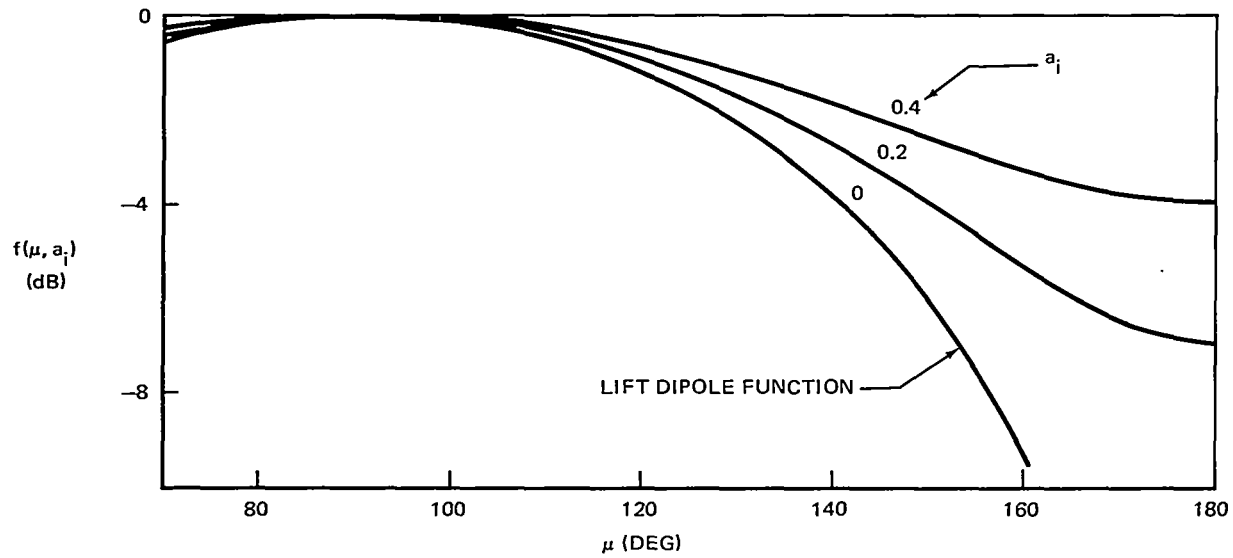

FIGURE 20. EFFECT OF SIDE-FORCE DIPOLE STRENGTH (a_i) ON THE SIDELINE NOISE FUNCTION

TABLE 3

DC-9-31 NORMALIZED OASPL MEASUREMENT AND PREDICTION

($\lambda = 90$ Degrees, $\mu = 90$ Degrees)

Configuration	OASPL From Flyover Measurements	OASPL From DA Method Prediction
A	125.8	130.4
B	134.0	133.4
C	134.5	– –
D	133.6	– –
E	136.3	132.2
F	137.4	135.4
G	138.4	134.7
H	138.6	136.0

values were used for locating the points where the solid lines of Figure 3 intersect the 100 m/s coordinate.

Fethney (Reference 12) has presented a few sideline data points for four different aircraft. His data indicate that the variation with the sideline angle is approximately like that of a monopole which, for constant radius, is invariant. The same result in the present notation would require $a_i = 1.0$, but for the DC-9-31 aircraft, a_i apparently ranges between 0 and 0.4. The reason for the different results is not understood.

In Reference 10, Figure 7, Fink presents sideline data obtained from flyover tests of the Convair 990 aircraft in the clean configuration. For the 200-Hz band, where airframe noise is expected to be dominant, the sideline noise variation is like that of a dipole. In contrast, for the 1600-Hz band where engine noise may be dominant, the sideline noise variation is like that of a monopole. Since engine noise would show the monopole variation, Fink concludes that the airframe noise alone must have the dipole variation.

In the past, some discussion has centered about the possibility of panel noise contributing to the sideline noise, but the authors have been unable to find any evidence of this phenomena.

Since turbulent flow over such a bluff device as a landing gear is known to generate fluctuating forces in a direction normal to the airplane plane of symmetry, the existence of a sideline dipole phenomena should be expected; such a dipole would not however be expected to be correlated with the aircraft lift dipole.

DRAG ELEMENT METHOD FOR AIRFRAME NOISE PREDICTION

The drag element (DE) method for airframe noise computation (Reference 5) is based on the subdivision of the airframe into seven elements or components whose noise is computed separately and then added antilogarithmically. The seven components are identified with the drag generated by each component; specifically these are:

1. Wing profile drag
2. Wing-induced drag
3. Fuselage drag
4. Nacelle drag
5. Horizontal tail drag
6. Landing gear drag
7. Leading edge slat drag

The method uses the assumption that there is no significant interaction between the various components.

The equation used to obtain the 1/3 OB spectrum for the jth component is

$$(SPL)_{1/3\ j} = OASPL_j + 10 \log (S(x))_j \tag{14}$$

where S is a spectral shape function of the nondimensional frequency x (see Equation (12) of Reference 5) where

$$x = f_b/f_{Stj} \tag{15}$$

and f_b is the band frequency and f_{Stj} is the spectrum peak frequency, where f_{Stj} is determined from

$$f_{Stj} = \frac{(Str)\, V_{TE}\,(j)}{d_{eq}\,(j)} \tag{16}$$

where the Strouhal number Str, trailing edge velocity V_{TE}, and the equivalent diameter d_{eq} are defined in Reference 5. Also, $OASPL_j$ is the OASPL for the jth component, computed from

$$OASPL_j = K_j + 10 \log F_j \tag{17}$$

where

$$F_j = \left(\frac{C_{Dj}}{C_{D_R}}\right)^n \left(\frac{S_j}{S_R}\right) \left(\frac{V_{TE}\,(j)}{V_R}\right)^m \left(\frac{h_R\, h}{R^2}\right)^2 \left(\frac{V}{V_R}\right)^6 \tag{18}$$

and C_{D_R} is a reference drag coefficient, S_R is a reference area, V_R is a reference speed, and h_R is a reference altitude, as given in Reference 5. Recommended values for the parameters K_j, S_j, n, m, and (V_{TE}/V) are given in Reference 5. A key parameter is the drag coefficient C_{Dj}; recommendations for estimating this parameter as a function of flap and slat deflection are given in Reference 5. Since n = 3 for all component calculations except the landing gear, the OASPL is rather sensitive to changes or small variations in C_{Dj}. Also, Equations (14) through (18) indicate that the SPLs vary like 60 log V, in contrast to the 50 log V relation (approximately) found in the preceding section. Since the method is based on constants derived from experimental data, the SPL level for any one particular airspeed could be made correct regardless of the power of V used in the method.

The DE method provides free-field SPL values, hence corrections must be added to Equation (14) to account for the effects of ground reflections in order that predictions of airframe noise can properly be compared with microphone measurements.

The coefficients used in the DA method have been obtained from the DC-10-10 flyover data in Reference 1. The parameter H (Equation (3)) for the DC-10-10, $6.38 \times 10^{11} s^4/m^2$, was used to obtain C_i's, as outlined on Pages [redacted] and [redacted]. Then, Equation (11) was used to compute OASPLs (see Table 4). The parameter $M^5 S_w p_a^2/(16\pi^2 R^2 p_o^2)$ used in Equation (5) is 3.23×10^{16}. Hence, the simple relation between C_i and the OASPLs for $\lambda = \mu = 90$ degrees is

$$OASPL = 10 \log(3.23 \times 10^{16} C_i^2) \qquad (19)$$

Predicted DC-9-31 normalized OASPLs are shown in Table 3. The differences between the predictions and the measurements are partly a result of measurement errors, but the main contribution to the differences is believed to be the result of geometric shape differences between the DC-10 and the DC-9 aircraft. In particular, the engine locations on the DC-10 are quite different from those of the DC-9. Perhaps interference effects between the wing and the pylons on the DC-10 is such as to cause noise sources of a type not found on the DC-9. This could be a reason that the predicted levels for Configuration A are higher than the measured levels.

Table 3 contains no prediction for Configurations C and D because no DC-10 data were taken with flaps up and slats extended, corresponding to Configurations C and D. The predictions for the DC-9 with 20- and 40-degree flap deflections were obtained by interpolating the DC-10 data obtained as the plane was flown with extensions of 0, 35, and 50 degrees.

TABLE 4

DC-9-31 GEOMETRIC PARAMETERS

Wing Area (S_W)	93.0 m^2
Wing Span (b)	28.4 m
Fuselage Length	32.6 m
Fuselage Diameter	3.35 m
Nacelle Length	5.2 m
Nacelle Diameter	1.5 m
Horizontal Tail Area	25.6 m^2
Plan Area of Both Pylons	4.8 m^2

Figures 21 through 28 show normalized SPL spectra for Configurations A through H. The data are compared with predictions made using both the DA and the DE methods.

The drag coefficients used in the DE method are given in Reference 6. The coefficients were determined from wind-tunnel model and flight tests of the aircraft. The coefficients are based on wing area; for use in the DE method, they must be based on the appropriate areas, as discussed in Reference 5. Pertinent parameters for this process are listed in Table 4. The leading edge slats have a chord equal to 13.8 percent of the wing chord. When extended, the slat drag coefficient based on slat area was assumed to be 0.025 because of the increase in the local velocity above the free-stream value caused by the slat extension. The extension also causes an increase of the wing profile drag. These two drag effects are shown in Reference 6 only as the total of the two effects. Since the DE method was developed to predict free-field SPLs whereas the DC-9 flyover measurements were taken with ground plane microphones, an increment of 6.0 dB was added to the DE results to account for ground reflections.

The comparisons for the clean configuration are shown in Figure 21. For frequencies above 200 Hz, the DE method matches the DC-9 data quite well; the DA method is a little high from 50 to 2000 Hz. Perhaps the large flap hinge fairings or the pylons on the DC-10 aircraft are responsible for added high-frequency noise which does not appear in the DC-9 data.

By using the method of Reference 10, the DC-9-31 normalized OASPL in the clean configuration is predicted to be 125.3 dB. The DE method gives 125.8 dB whereas the DC-9 measured data also give

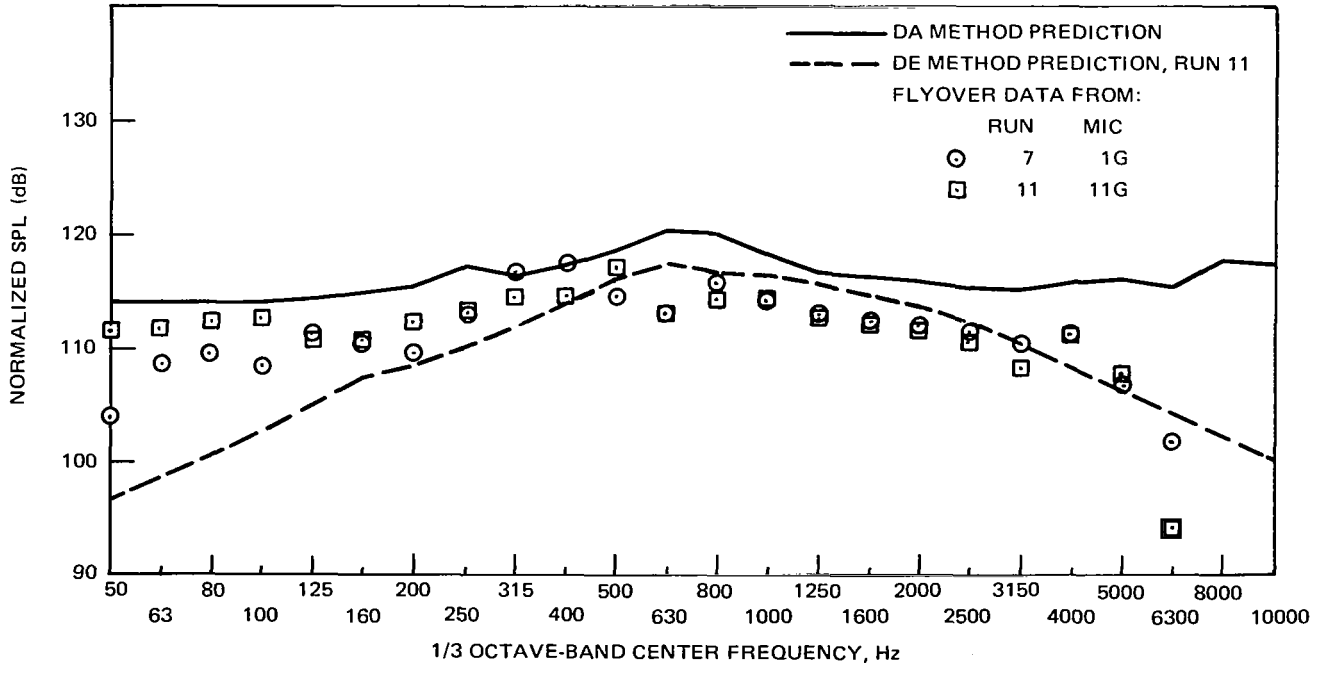

FIGURE 21. NORMALIZED SPL'S FOR CONFIGURATION A

125.8 dB. In contrast, the DA method gives 130.4 dB. Hence, the method of Reference 10 and the DE method agree with the data.

Figure 22 shows that the clean configuration with gear down is not well predicted by the DE method. Apparently, more work needs to be done on this method to account for the gear effect. The DA method slightly underpredicts the DC-9 data, probably because the gear-effect coefficients were obtained from DC-10 data with flaps deflected 35 degrees, where the drag effect of the gear is reduced somewhat by the effects of the flap deflection. No data runs were made with the DC-10 in the flaps-up gear-down configuration.

Figures 23 and 24 represent Configurations C and D, respectively. Since no DC-10 data were taken with these configurations, the DA method could not be used for Figures 23 and 24. Again, the DE method predicts well at frequencies of 400 Hz and above, but it underpredicts the low frequencies for the gear-up configuration and overpredicts the landing gear noise.

Figures 25 through 28 represent the flap-down configurations. Since the DC-10-10 slats extend automatically whenever the flaps are down, the DA method has a slat effect included for all flaps-down configurations. For these configurations, the DA method is either a little low or approximately correct for frequencies of 1000 Hz and above, but at the lower frequencies, where the SPLs are apparently controlled by flap noise, the DA method predictions are on the order of 5 to 7 dB too low. The DE method is a little low for frequency bands near 400 Hz in Figure 25, the 20-degree flap case. For the 50-degree flap cases shown in Figures 27 and 28, the DE method overpredicts at low frequencies and underpredicts at intermediate and high frequencies. The same trend prevails, but to a lesser degree, in the 40-degree flap case, as shown in Figure 26.

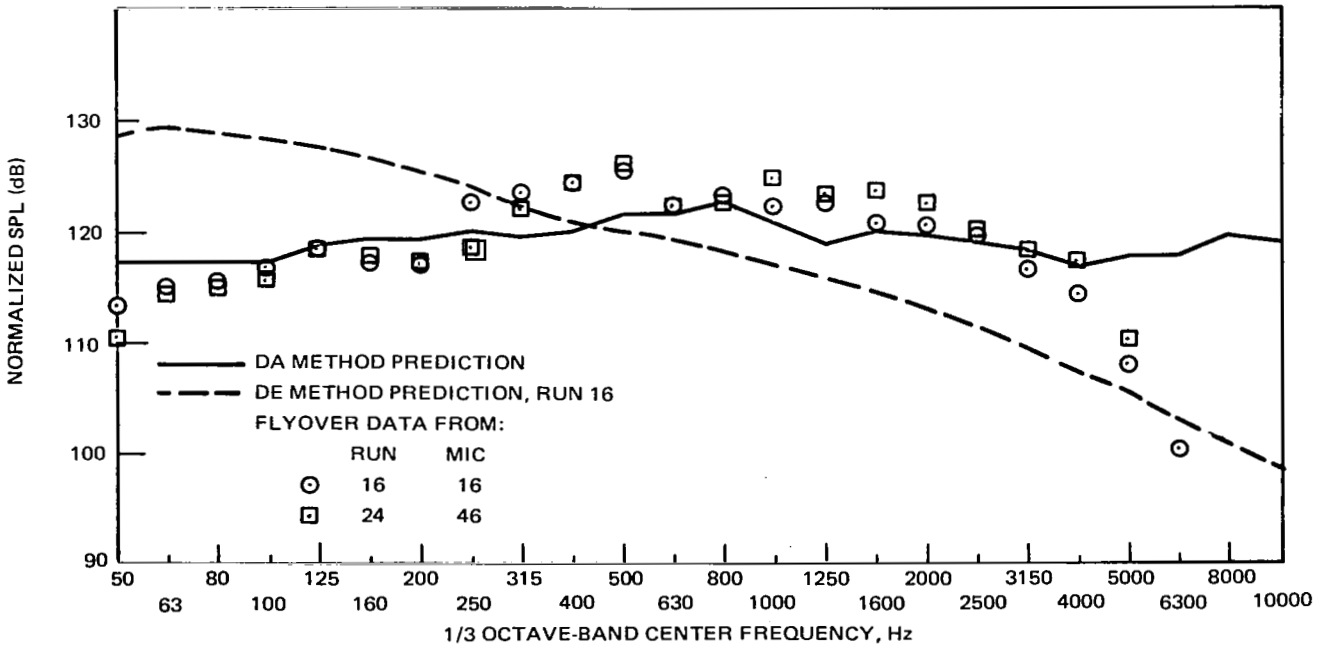

FIGURE 22. NORMALIZED SPL'S FOR CONFIGURATION B

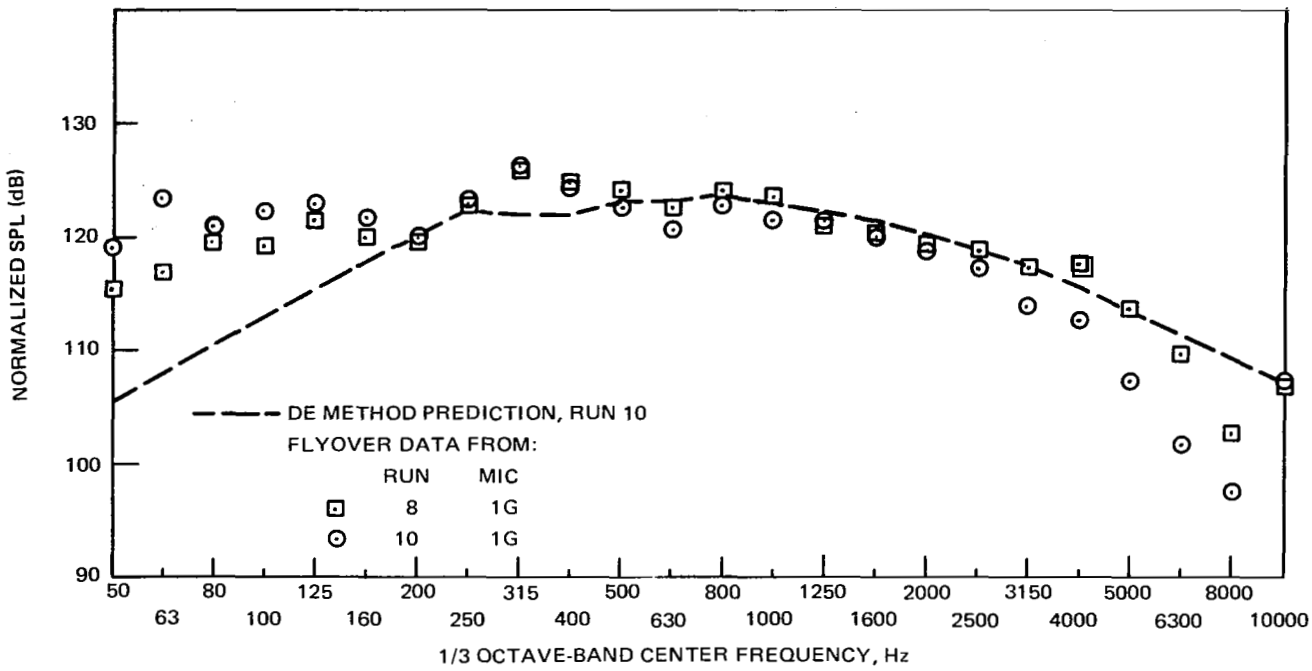

FIGURE 23. NORMALIZED SPL'S FOR CONFIGURATION C

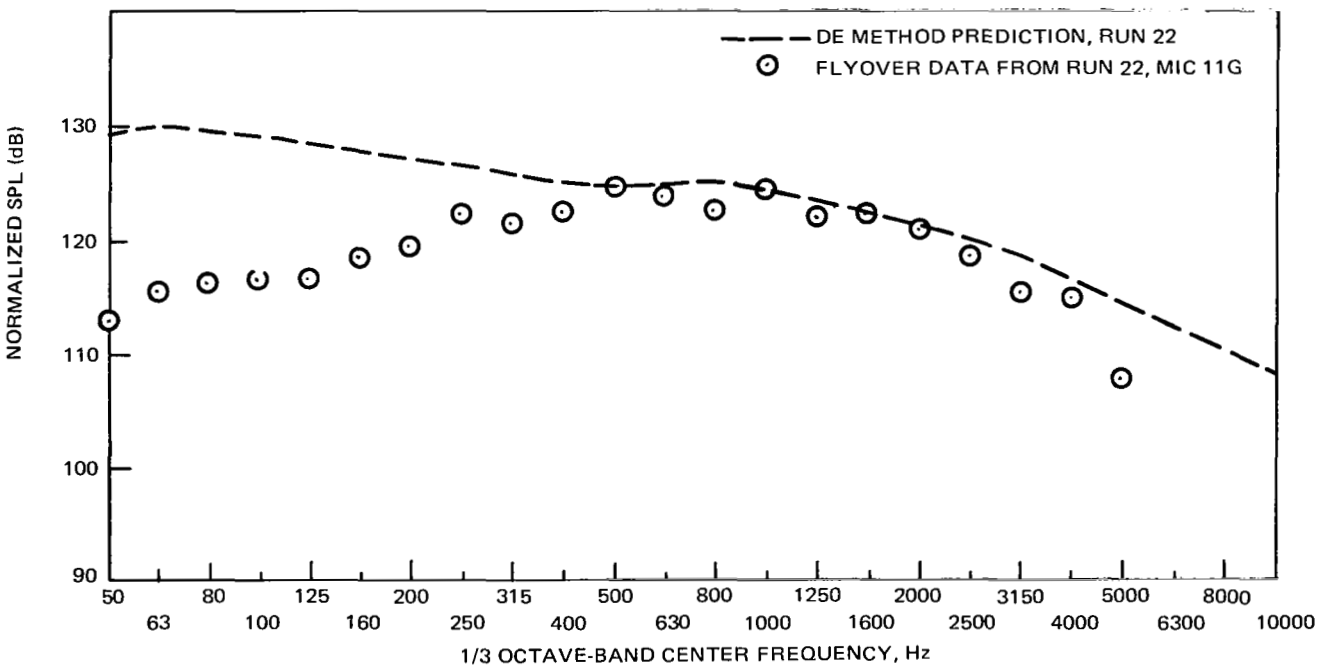

FIGURE 24. NORMALIZED SPL'S FOR CONFIGURATION D

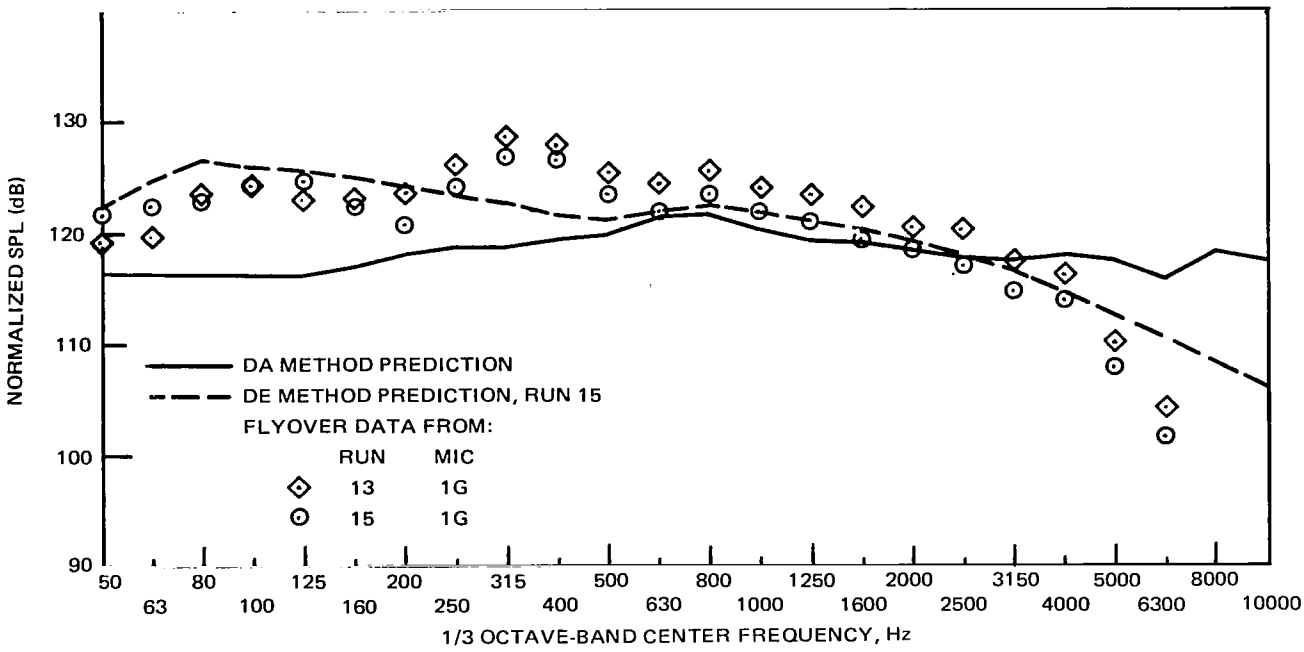

FIGURE 25. NORMALIZED SPL'S FOR CONFIGURATION E

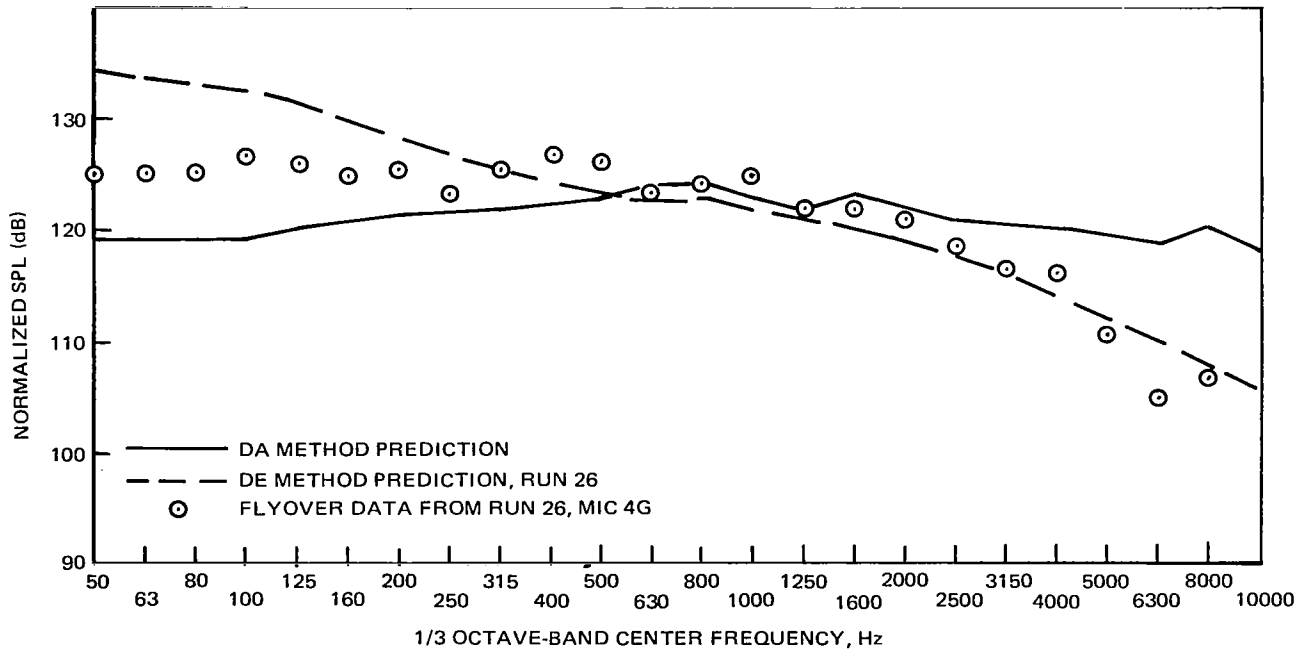

FIGURE 26. NORMALIZED SPL'S FOR CONFIGURATION F

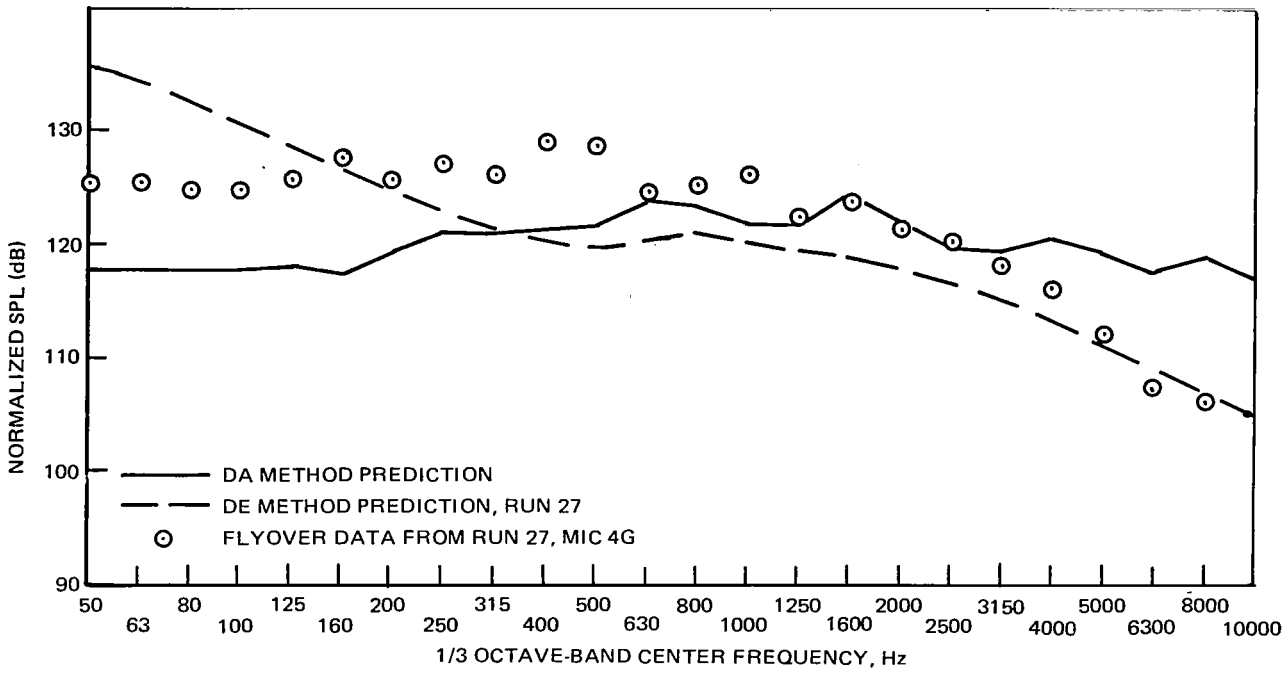

FIGURE 27. NORMALIZED SPL'S FOR CONFIGURATION G

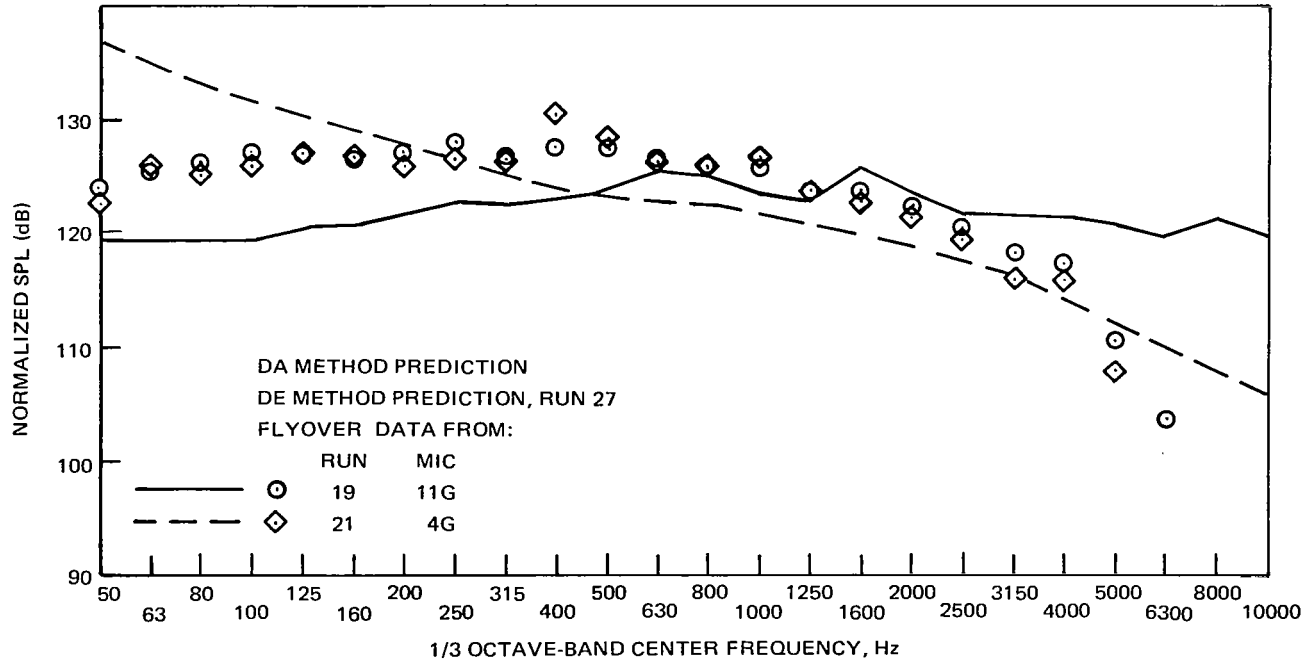

FIGURE 28. NORMALIZED SPL'S FOR CONFIGURATION H

CONCLUSIONS AND RECOMMENDATIONS

The DC-9-31 airframe noise measurements reported on in this document are believed to be valid up to a frequency of approximately 3150 Hz; above this frequency, engine noise is a significant factor in the data, but is not large enough to change overall sound pressure levels by a significant amount.

An analysis of the DC-9 flyover data indicates that both lift and drag dipoles exist as a significant part of the DC-9 airframe data. A side-force dipole of significant strength apparently exists only for the flaps-down gear-down configurations, but its strength is less than that of the lift dipole.

The DC-9 airframe noise data vary approximately as the fifth power of the flight velocity.

The airframe noise for the clean configuration is much lower than that with either the gear or the slats extended. A surprising feature is that the extension of both the gear and the slats caused no more noise than the extension of the gear or the slats alone. The airframe noise with the flaps extended is significantly greater than that for the configurations with either the gear or the slats extended separately.

The drag element method was successful in predicting DC-9 airframe noise for the clean configuration, but the method needs improvement for predicting the effects of flap deflection and landing gear extension.

The data analysis method used in this paper, which is a scaling of DC-10-10 data to the DC-9 airplane configuration, predicted overall sound pressure noise levels about 4 dB greater than the measured data for the clean aircraft configuration, but the prediction was essentially correct for the flaps-up gear-down configuration. For all four configurations with flaps down, the predictions are slightly below the data for frequencies of 1000 Hz and greater, but at lower frequencies, the predictions are on the order of 5 to 7 dB too low.

In order to facilitate airframe noise comparisons of different aircraft, nondimensional coefficients such as those given in Equation (11) should be used to describe airframe noise. Then Equation (11) can be used to obtain sound pressure levels for a specific application.

The method from Reference 10, as well as the drag element and the data analysis methods, should be investigated as promising means of predicting airframe noise.

REFERENCES

1. Munson, A. G., A Modeling Approach to Nonpropulsive Noise, AIAA Paper 76-525, July 1976.

2. Healy, G. J., Measurement and Analysis of Aircraft Far-Field Aerodynamic Noise, NASA CR-2377, 1974.

3. Gibson, J. S., Nonengine Aerodynamic Noise Investigation of a Large Aircraft, NASA CR-2378, 1974.

4. Hardin, J. C., Fratello, D., Hayden, R. E., Kadman, Y., and Africk, S., Prediction of Airframe Noise, NASA TN D-7821, February 1975.

5. Revell, J. D., Healy, G., and Gibson, J., Methods for the Prediction of Airframe Aerodynamic Noise, AIAA Paper No. 75-539, March 1975.

6. Bauer, A. B., and Munson, A. G., DC-9-31 Airframe Noise Data, Douglas Aircraft Company Report Number MDC-J4583, December 1977.

7. SAE Committee A-21, Standard Values of Atmospheric Absorption as a Function of Temperature and Humidity, SAE Aerospace Recommended Practice, ARP 866A, revised March 1975.

8. Morgan, H. G., and Hardin, J. C., Airframe Noise - The Next Aircraft Noise Barrier, AIAA Paper No. 74-949, August 1974; also see J. Aircraft, Vol. 12, July 1975, p. 622.

9. Fink, M. R., Approximate Prediction of Airframe Noise, J. Aircraft, Vol. 13, November 1976, p. 833.

10. Fink, M. R., Airframe Noise Prediction Method, DOT/FAA Report FAA-RD-77-29, March 1977.

11. King, W. F., The Effect of Motion on Acoustic Dipole Models for Aerodynamic Noise Prediction, Physics Letters, Vol. 62A, Number 4, August, 1977, pp. 282-284.

12. Fethney, P., An Experimental Study of Airframe Self-Noise, Aeroacoustics STOL Noise; Airframe and Airfoil Noise, Vol. 45, Progress in Aeronautics and Astronautics, M.I.T. Press, Cambridge, Mass., 1976, pp. 379-403. Also, AIAA Paper 75-511, March 1975.

APPENDIX

THE CALCULATION OF COEFFICIENTS FOR THE DATA ANALYSIS METHOD OF AIRFRAME NOISE PREDICTION

Two different procedures are available for the calculation of the coefficients for the DA method of noise prediction. The methods may be applied either to aircraft OASPLs or to any one or combination of several 1/3 octave band SPL data.

The first method follows:

1. Using Equations (9) and (11) and the condition $\lambda = \mu = 90$ degrees, calculate C_i to match the normalized flyover data for a specific configuration of the aircraft.

2. Using a plot of the normalized flyover data versus λ for the condition $\mu = 90$ degrees, solve Equation (11) to find the value of B_i needed to match the data slope in the neighborhood of $\lambda = 90$ degrees. Then find the value of A_i needed for the best match to the data for values of λ far away from 90 degrees.

3. Using a plot of the normalized flyover data versus μ for the condition $\lambda = 90$ degrees, solve Equation (11) to find the value of a_i needed for the best match to the data for values of μ far away from 90 degrees.

4. For any different configuration of the aircraft, repeat Steps 1 to 3.

The second method is derived from the two-dipole method of Reference 1. First, the function $g(\lambda)$ is obtained from aircraft flyover noise data

$$g(\lambda) = \overline{p_s^2}\,(1 - M_r)^4 R^2 \qquad \text{(A-1)}$$

As explained in Reference 1, the function is defined for $\lambda = 0$ to 180 degrees and is cyclic with 180-degree periods. Also, $g(\lambda)$ is represented by the Fourier series:

$$g(\lambda) = D_0 + D_2 \cos 2\lambda + E_2 \sin 2\lambda + \ldots \qquad \text{(A-2)}$$

where the coefficients are obtained from

$$D_o = \frac{1}{2\pi} \int_o^{2\pi} g(\lambda)\, d\lambda \tag{A-3}$$

$$D_m = \frac{1}{\pi} \int_o^{2\pi} g(\lambda) \cos(m\lambda)\, d\lambda \text{ for } m > 0 \tag{A-4}$$

$$E_m = \frac{1}{\pi} \int_o^{2\pi} g(\lambda) \sin(m\lambda)\, d\lambda \tag{A-5}$$

then,

$$F_L = \frac{16\,\pi^2\, a_o^2\, (D_o - D_2)}{V^6\, p_o^2} \tag{A-6}$$

$$F_D = \frac{16\,\pi^2\, a_o^2\, (D_o + D_2)}{V^6\, p_o^2} \tag{A-7}$$

$$F_{LD} = \frac{16\,\pi^2\, a_o^2\, D_2}{V^6\, p_o^2} \tag{A-8}$$

and

$$F_\ell = \left(\frac{16\,\pi^2\, (D_o - D_2)}{S_w\, M^5\, p_a^2} \right)^{1/2} \tag{A-9}$$

$$F_d = \left(\frac{16\,\pi^2\, (D_o + D_2)}{S_w\, M^5\, p_a^2} \right)^{1/2} \tag{A-10}$$

$$F_{\ell d} = \left(\frac{16\,\pi^2\, E_2}{S_w\, M^5\, p_a^2} \right)^{1/2} \tag{A-11}$$

Note that $\overline{p_s^2}$ is the sound pressure squared for any given one-third octave band. Alternately, $\overline{p_s^2}$ may be taken as the overall sound pressure squared, and then the above six coefficients are K_L, D_D, K_{LD}, K_ℓ, K_d, $K_{\ell d}$, respectively.

The two methods are both so new that it is too early to make any specific recommendations as to which method may be preferred for any given problem. It is expected that both methods will give essentially the same results.

1. Report No.	2. Government Accession No.	3. Recipient's Catalog No.
NASA CR-3027		

4. Title and Subtitle	5. Report Date
Airframe Noise of the DC-9-31	July 1978
	6. Performing Organization Code

7. Author(s)	8. Performing Organization Report No.
A. B. Bauer and A. G. Munson	
	10. Work Unit No.
	505-06-23-01
9. Performing Organization Name and Address	11. Contract or Grant No.
Douglas Aircraft Company 3855 Lakewood Boulevard Long Beach, CA 90846	NAS1-14696
	13. Type of Report and Period Covered
	Contractor Report
12. Sponsoring Agency Name and Address	14. Sponsoring Agency Code
National Aeronautics and Space Administration Washington, DC 20546	

15. Supplementary Notes

Langley Technical Monitor: Jay C. Hardin

Final Report

16. Abstract

Airframe noise measurements are reported for the DC-9-31 aircraft flown at several speeds and with a number of flap, landing gear, and slat extension configurations. The data are corrected for wind effects, atmospheric attenuation, and spherical divergence, and are normalized to a one-meter acoustic range. The sound pressure levels are found to vary approximately as the fifth power of flight velocity. Both lift and drag dipoles exist as a significant part of the airframe noise. The sideline data imply that a significant sideforce dipole exists only for the flap and gear down condigurations; for other configurations the data imply the existence of only the lift and drag dipoles. The data are compared with airframe noise predictions using the drag element and the data analysis methods. Although some of the predictions are good, further work is needed to refine the methods, particularly for the gear-down and flaps-down configurations.

17. Key Words (Suggested by Author(s))	18. Distribution Statement
Airframe Noise, Non-propulsive Noise, Noise Prediction	Unclassified - Unlimited Subject Category 71

19. Security Classif. (of this report)	20. Security Classif. (of this page)	21. No. of Pages	22. Price*
Unclassified	Unclassified	53	$5.25

* For sale by the National Technical Information Service, Springfield, Virginia 22161

NASA-Langley, 1978